5-2012

Numerical simulation of phase change material composite wallboard in a multi-layered building envelope.

Stephen David Zwanzig
University of Louisville

NUMERICAL SIMULATION OF PHASE CHANGE MATERIAL COMPOSITE WALLBOARD IN A MULTI-LAYERED BUILDING ENVELOPE

By
Stephen David Zwanzig
B.S. Mechanical Engineering, University of Louisville, 2011
B.S. Mathematics, University of Louisville, 2007

A Thesis
Submitted to the Faculty of the
University of Louisville
J.B. Speed School of Engineering
As Partial Fulfillment of the Requirements
For the Professional Degree

MASTER OF ENGINEERING

Department of Mechanical Engineering

May 2012

NUMERICAL SIMULATION OF PHASE CHANGE MATERIAL COMPOSITE WALLBOARD IN A MULTI-LAYERED BUILDING ENVELOPE

Submitted by:_____
Stephen David Zwanzig

A Thesis Approved On

_____
(Date)

by the Following Reading and Examination Committee:

_____
Yongsheng Lian, Thesis Director

_____
Ellen G. Brehob, Thesis Co-Director

_____
William M. McGinley

_____
M. Keith Sharp

ACKNOWLEDGEMENTS

First, a special thanks to my advisors Dr. Yongsheng Lian and Dr. Ellen G. Brehob for sharing their knowledge of numerical modeling and heat transfer and for the continuous support and guidance they provided over the course of this study. I would also like to thank Jeff Kiesel and Dr. William M. McGinley for motivating me through numerous discussions and a shared interest in phase change material research.

Finally, I would like to acknowledge the partial support from the U.S. DOE Higher Education Experiences at Oak Ridge National Laboratory administered by ORISE and the Conn Center for Renewable Energy and Energy Efficiency.

ABSTRACT

Residential buildings account for a large portion of total energy consumption in the United States. Residential energy usage can be dramatically reduced by improving the efficiency of building envelope systems. One such method is to incorporate thermally massive construction materials into the building envelope. This benefits building operation by reducing the energy requirement for maintaining thermal comfort, downsizing the AC/heating equipment, and shifting the time of the peak load on the electrical grid. Phase change materials (PCMs) are promising material for that purpose. When impregnated or encapsulated into wallboard or concrete systems, PCMs can greatly enhance their thermal energy storage capacity and effective thermal mass. In this work, a numerical study is conducted to investigate the characteristics of PCMs in building applications. For that purpose a one-dimensional, transient heat equation for a multi-layered building envelope is solved using the Crank-Nicolson scheme. The effect of PCM is modeled with a latent heat source term. The code also incorporates sun loading and uses real weather data. Using this code a PCM composite wallboard incorporated into the walls and roof of a residential building was examined. The PCM performance was studied under all seasonal conditions using TMY3 data for exterior boundary conditions. Comparisons were made between different PCM wallboard locations. This work shows that there is an optimized location for PCM placement within building envelope and the location depends on the thermal resistance of the layers between the PCM and the exterior boundary. The energy savings potential was identified by comparing the performance of the PCM wallboard with the performance of a building envelope without

PCM. This work shows that a PCM composite wallboard enhanced building can reduce the annual cooling load from the walls by as much as 19.7% and from the roof by as much as 8.1%. Similarly, the annual heating loads can be reduced by as much as 6% and 6.4% for the walls and roof respectively. It was also shown that the peak electricity load can be shifted by as much as three hours in the summer for a south facing wall. Studies are also conducted to compare the PCM performance across three climate zones. This work shows that PCM performance varies significantly across these zones.

TABLE OF CONTENTS

NOMENCLATURE

A	=	coefficient corresponding to the west node
A_f	=	face area of control volume (m^2)
A_i	=	anisotropy index
a	=	coefficient associated with unknown values
B	=	coefficient corresponding to the node in question
b	=	coefficient associated with known values
C	=	coefficient corresponding to the east node
CV	=	control volume
C_{amt}	=	cloud amount (tenths)
c_p	=	specific heat (kJ kg^{-1} K^{-1})
D	=	coefficient corresponding to values at the previous time step
E	=	equation of time (hr)
F	=	view factor
Fo	=	Fourier number
f	=	Crank-Nicolson weighting factor (0, 0.5, or 1) or modulating factor
G_{sc}	=	solar constant (W m^{-2})
g	=	liquid phase fraction
H	=	enthalpy (kJ kg^{-1})
h	=	heat transfer coefficient (radiation/convection)
I	=	total incident radiation (MJ m^{-2})
k	=	thermal conductivity (W m^{-1} K^{-1})
L	=	latent heat of fusion (kJ kg^{-1})
L_{loc}	=	local longitude (degrees)
L_{st}	=	standard meridian (degrees)
n	=	day of the year
Q	=	incident radiation (W m^{-2})
R_b	=	beam ratio
T	=	Temperature (°C or K)
t	=	time (s or h)
V	=	volume (m^3)
W	=	mass fraction
x	=	spatial coordinate (m)

Greek Symbols

α	=	thermal diffusivity (m^2/s)
β	=	air-sky attenuation factor or surface tilt angle
γ	=	surface azimuth angle (degrees)
γ_s	=	solar azimuth angle (degrees)
δ	=	nodal spacing or declination angle (degrees)
ε	=	emissivity
θ	=	angle of incidence (degrees)
θ_z	=	zenith angle (degrees)
ρ	=	density

ρ_g	=	ground reflectance
σ	=	Stefan Boltzmann constant
φ	=	volume fraction or local latitude (degrees)
ω	=	hour angle (degrees)

Subscripts

0	=	initial
b	=	beam
c	=	composite
d	=	diffuse
dewp	=	dew point
E	=	east node
e	=	interface between node P and E
gnd	=	ground
gyp	=	gypsum wallboard
IR	=	infrared radiation
i	=	room interior
l	=	liquid
o	=	extraterrestrial radiation
P	=	central node (node in question)
r	=	radiative
s	=	solid
T	=	total radiation on a tilted surface
W	=	west node
w	=	interface between node P and W

Superscripts

m	=	iteration level
n	=	current time step

LIST OF TABLES

LIST OF FIGURES

I. INTRODUCTION

A. Overview

The residential sector accounts for a large portion of total energy consumption in the United States. According to a 2010 study by the U.S. Energy Information Administration, residential buildings use nearly 22.6% of the yearly total energy consumed in the US (EIA, 2010). Furthermore, approximately 51.7% of this residential energy was for heating and cooling (EIA, 2005). Residential energy usage can be dramatically reduced by improving the efficiency of building envelope systems. One such method is to incorporate thermally massive construction materials into the building envelope. The addition of thermal mass allows the building envelope to become an effective thermal energy storage system. A well designed building envelope thermal energy storage system can improve building operation by reducing the energy required to maintain thermal comfort, downsizing the AC/heating equipment, and shifting the time of the peak load on the electrical grid.

Thermal energy storage can be achieved using either sensible or latent heat storage mechanisms. Sensible heat storage is quantified as the amount of heat stored or released by a material through a temperature change. Latent heat storage is the amount of heat stored or released during a process that occurs with little change in temperature. A benefit of latent heat storage over sensible is that latent heat storage occurs in a narrow phase change temperature range, resulting in a small change in temperature associated with a large amount of energy storage. Figure 1 compares the temperature change

required by three materials to store 300 kJ of energy per unit mass (measured from a base temperature of 0°C). It is clear that the PCM, n-Octadecane, has the lowest temperature variation while concrete has the highest.

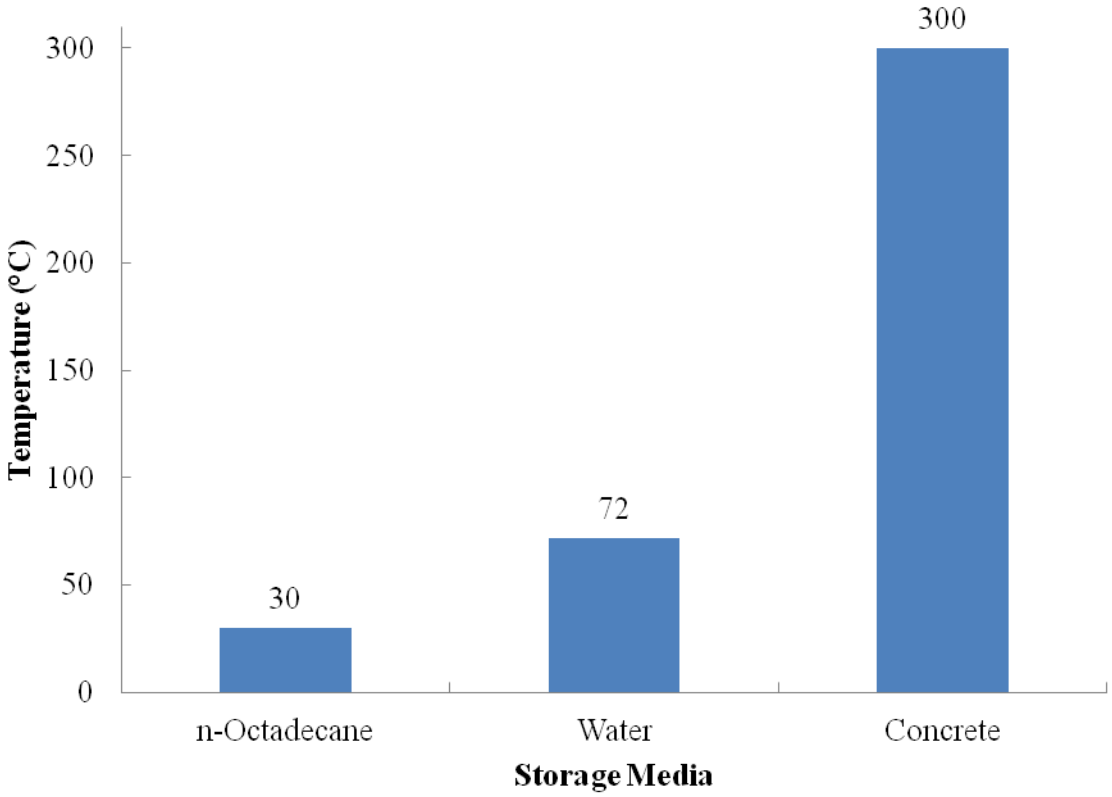

FIGURE 1 – Temperature Increase Needed to Store 300 kJ of Energy Per Unit Mass Material

Given this higher energy storage potential per unit mass it is clear that thermal energy storage systems that incorporate PCMs require much smaller volumes compared to more conventional materials.

B. Characteristics of PCMs

In the design of a thermal energy storage system the PCM must be carefully chosen. The thermal, physical, chemical, and economic properties of PCM materials all require special consideration (Zalba et al., 2003). The thermal properties of the PCM should be selected to ensure that the phase change temperature is appropriate to the application, ensuring a high change of enthalpy near the desired temperature of use. Also, high thermal conductivity in both solid and liquid states is preferable. The important physical properties desired are high density, low variations in density between phases, and minimal undercooling. (Undercooling represents the cooling of the liquid phase to a temperature below its freezing point without solidification or crystallization occurring). The chemical properties of a successful PCM candidate should guarantee the long term stability of the material and ensure that no phase separation occurs during thermal cycling. (Phase separation is the separation of liquid phases which contain different concentrations of shared components). Finally, the material should be cheap, abundant, and recyclable. Several review papers provide details of the properties of candidate materials for use as PCMs in buildings (Farid et al., 2004; Zalba et al., 2003; Kuznik et al., 2011).

The candidate materials for use in thermal energy storage systems in buildings can be classified as either organic or inorganic materials. The class of organic PCMs includes paraffins, fatty acids, and polyethylene glycol. The advantages of organic PCMs include (Kuznik et al., 2011; Zalba et al., 2003):

- Availability in a large melting temperature range

- low or no undercooling
- non-corrosive
- chemical and thermal stability (no phase separation)
- congruent melting
- compatibility with conventional construction materials
- recyclable

The disadvantages of organic PCMs include (Kuznik et al., 2011; Zalba et al., 2003):

- low thermal conductivity
- flammability
- lower phase change enthalpy than inorganic

The class of inorganic PCMs is composed of salt hydrates. The advantages of inorganic PCMs include (Kuznik et al., 2011; Zalba et al., 2003):

- greater phase change enthalpy than organic
- low cost and easy availability
- sharp phase change temperature range
- high thermal conductivity
- non-flammable

The disadvantages of inorganic PCMs are (Kuznik et al., 2011; Zalba et al., 2003):

- large volume change
- undercooling
- corrosive
- poor thermal stability
- phase separation

Table I below lists some previously studied organic and inorganic PCMs and their material properties (Zalba et al., 2003).

TABLE I

ORGANIC AND INORGANIC PCM CANDIDATES AND MATERIAL PROPERTIES

Compound	Class	Melting temp (°C)	Heat of fusion (kJ/kg)	Thermal conductivity (W/mK)	Density (kg/m^3)
Polyglycol E400	Organic	8	99.6	0.187 (liquid, 38.6°C)	1125 (liquid, 25°C) 1228 (solid, 4°C)
Paraffin C_{13}-C_{24}	Organic	22-24	189	0.21 (solid)	760 (liquid, 70°C) 900 (solid, 20°C)
Paraffin C_{18}	Organic	27.5	243.5	0.148 (liquid, 40°C) 0.358 (solid, 25°C)	774 (liquid, 70°C) 814 (solid, 20°C)
Capric acid	Organic	32	152.7	0.153 (liquid, 38.5°C)	878 (liquid, 45°C) 1004 (solid, 24°C)
Paraffin C_{16}-C_{28}	Organic	42-44	189	0.21 (solid)	765 (liquid, 70°C) 910 (solid, 20°C)
$LiClO_3$-$3H_2O$	Inorganic	8.1	253	n.a.	1720
$Mn(NO_3)_2$-$6H_2O$	Inorganic	25.8	125.9	n.a.	1728 (liquid, 40°C) 1795 (solid, 5°C)
$CaCl_2$-$6H_2O$	Inorganic	29	190.8	0.54 (liquid, 38.7°C) 1.088 (solid, 23°C)	1562 (liquid, 32°C) 1802 (solid, 24°C)
Na_2SO_4-$10H_2O$	Inorganic	32.4	254	0.544	1485 (solid)
$Zn(NO_3)_2$-$6H_2O$	Inorganic	36.4	147	0.469 (liquid, 61.2°C)	1937 (solid, 24°C)

The main advantages of inorganic PCMs as compared to organic are the higher heat of fusion, higher thermal conductivity, and inflammability. However, from Table I it is clear that the difference in the heat of fusion values between organic and inorganic compounds, in the temperature ranges reported, are not disparate enough to eliminate organic PCMs as thermal energy storage system candidates. Also shown in Table I, the thermal conductivities of inorganic PCMs are significantly higher than those of organic PCMs. This high thermal conductivity is a desirable trait in that it allows the PCM to quickly absorb or release heat, facilitating a timely phase transition. However, the

incorporation of PCMs into the building envelope typically requires the mixing of the PCM with a building material such as lightweight concrete or gypsum wallboard which have thermal conductivities of 0.1 – 0.3 W/mK and 0.17 W/mK respectively (Incropera et al., 2007). Given that the thermal conductivities of the PCM and the medium carrying the PCM are of the same order of magnitude, this disadvantage of low thermal conductivity found in the organic PCMs is overcome through proper implementation. Several techniques have been developed to overcome the flammability of organic PCMs. The use of brominated paraffins results in a product that is self-extinguishing. Also, the sequential treatment of plasterboard, first in PCM and then in an insoluble liquid fire retardant can provide a self-extinguishing building envelope material (Khudhair and Farid, 2004).

The organic PCMs generally outperform the inorganic variety with respect to thermal stability and undercooling. Studies have shown that organic paraffins have good thermal stability because neither thermal cycling nor contact with metals degrades their thermal behavior (Farid et al., 2004). Also, paraffins display self-nucleating properties which limit the extent of undercooling that occurs during the solidification stage.

Another notable advantage of organic paraffins is their thermo-adjustability. This property allows alterations of the phase change temperature through the manipulation of PCM composition. It is possible to vary the number of carbon atoms or form different molecular alloys which allow a continuous variation of the phase change temperature within certain ranges (Zalba et al., 2003).

Finally, commercial paraffins, as opposed to technical grade varieties, are relatively cheap (Farid et al., 2004), exhibit reasonable storage densities over a wide range of melting temperatures, display negligible undercooling, and are thermally and chemically stable. These properties make paraffins the ideal candidate for usage in thermal energy storage systems integrated into the building envelope.

C. Application Techniques

In light of the benefits listed above, the use of PCMs for thermal energy storage in building envelopes has drawn growing interest. To explore the benefits associated with the latent heat storage of PCMs, different techniques have been developed to incorporate the PCMs into the building envelope.

The most forthright technique is the direct impregnation of porous building materials with the PCM. The most common building materials that use this technique are gypsum wallboard and concrete. Gypsum wallboard is an ideal candidate given that approximately 41% of the wallboard volume is air voids (Khudhair and Farid, 2004). After impregnation, the gypsum matrix structure transfers the heat to the PCM impregnated in the pores of the matrix. However, this technique can suffer from leakage issues where the impregnated PCM leaks out of the matrix during thermal cycling (Kuznik et al., 2011).

A second technique is the micro- or macro-encapsulation of the PCMs prior to incorporating them into the building materials. This solves the problem of PCM leakage by fully containing the PCM in some kind of encapsulate. The micro-encapsulation of

octadecane in waterborne polyurethane is described by Kim and Kim (2004) in which spheres of 1-6 μm diameter with octadecane cores were produced. The microcapsules form a powder which can be mixed in with a building material such as gypsum wallboard or concrete during casting. Figure 2 shows a commercial microencapsulated PCM in a gypsum wallboard matrix.

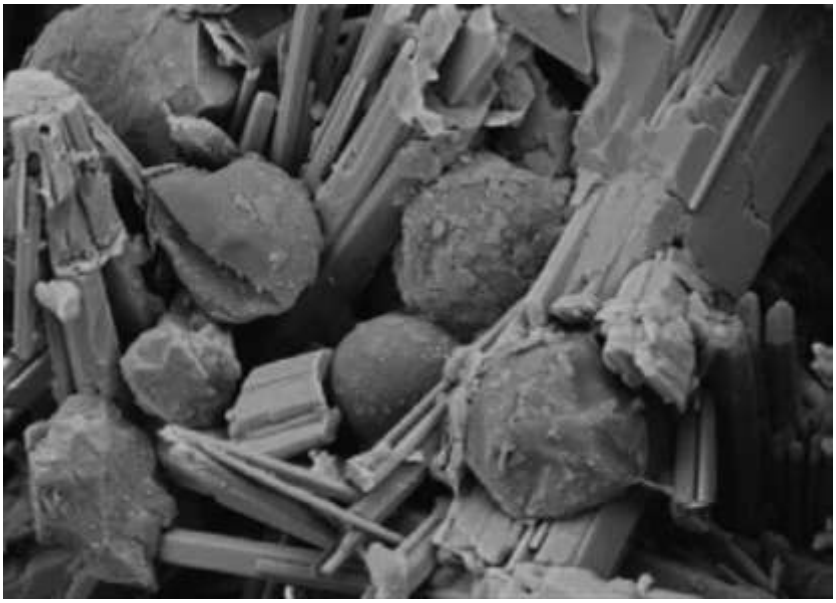

FIGURE 2 – Micronal PCM® in Gypsum Wallboard Matrix (BASF, 2009)

Macro-encapsulation can be achieved in many ways. Research has been done where various PCMs have been incorporated into rigid plastic and steel containers of varying shapes and sizes and then incorporated into the building structure (Kuznik et al., 2011).

A third technique that has been developed is the use of shape-stabilized PCM forms. These forms are created from a liquid mixture of the PCM and a support material. The mixture is used at temperatures below the solidification temperature of the support material, but at temperatures which allow the PCM to go through the liquid-solid phase transition. In this way the PCM is contained within the support material that provides the mixture with structural stability. Shape stabilized paraffin has been created in this way consisting of 74% paraffin and 26% high-density polyethylene (Zalba et al., 2003).

D. Studies of PCMs in Buildings

Studies have found that incorporating PCM into building envelopes can reduce energy consumption and smooth indoor temperature swings. Diaconu and Cruceru (2010) studied a composite PCM wall system in which PCM impregnated gypsum board was placed on both the interior and exterior of the wall. A numerical method was used to solve the transient heat equation and the enthalpy method was incorporated to account for the thermo-physical properties of the composite PCM wallboard. They found a peak cooling load reduction of 35.4%, peak heating load reduction of 35.4%, total cooling load reduction of 1%, and a 12.8% value of heating energy savings. Athienitis et al. (1997) studied a PCM enhanced gypsum board that was soaked in liquid butyl stearate which has a phase change temperature range of 16.0-20.8°C. The wallboard contained about 25% by weight butyl stearate. Full-scale experiments were conducted in which an outdoor test-room containing PCM lined interior walls was studied during the cooling season in Montreal, Quebec. The indoor temperature was allowed to float without any temperature

control from an A/C unit during the cooling season. During the heating season, a heating system would deliver heat if the controlled temperature was at least half a degree lower than the desired set point. They showed that the PCM enhanced wallboard can reduce the maximum room temperature by about 4°C, significantly reducing overheating. Additionally, they found the PCM enhanced wallboard can potentially reduce the total heating load by 15%. In their study, the thermal properties of the PCM wallboard were determined using Differential Scanning Calorimetry (DSC) and then incorporated into a one-dimensional numerical model. The simulation results agreed closely with experimental data.

Stovall and Tomlinson (1995) studied a PCM enhanced gypsum board. They developed a gypsum wallboard impregnated with a paraffin mixture that was primarily n-octadecane. They showed that the wallboard could be manufactured containing as much as 30% PCM by weight. Their simulation showed that a PCM enhanced building envelope had significant load management potential with essentially no energy penalty associated with its implementation.

Another attractive property associated with PCM's is that they can potentially reduce the peak electrical load as well as shift the peak load to a later time, thereby reducing the electrical grid demand.

Cabeza et al. (2007) conducted an experimental study of micro-encapsulated PCM incorporated into concrete. Identical concrete cubicles were constructed in Llieda, Spain, one being composed of concrete impregnated with Micronal PCM® (BASF, 2008)

and one being composed of pure concrete. The cubicles did not use any indoor climate control, allowing the indoor temperatures to float freely. During the summer the PCM cubicle achieved a reduction in maximum indoor temperatures of about 1°C with a 2 hour shift in peak load.

In another study Halford and Boehm (2007) performed a numerical study addressing the potential for peak load shifting using encapsulated PCM. A one-dimensional model was developed with sinusoidal temperature boundary conditions representing the diurnal cycle. A 19-57% reduction in peak load was found to occur with the addition of a PCM layer to a conventionally insulated wall. It was also found that significant load shifting was at least theoretically possible.

E. Phase Change Material Characterization

1. Property Measurement

One of the challenges in the study of PCMs is to develop an accurate prediction of the thermal properties of the material, which is required for accurate modeling and performance evaluation. To this end the enthalpy as a function of temperature of the PCM must be known. The most common measurement method for achieving this is differential scanning calorimetry (Kuznik et al., 2011). There are two kinds of DSC machines, a power compensating DSC and a heat flux DSC. (Only the heat flux DSC will be discussed here). Heat flux DSC is a technique in which a sample material and a reference material are enclosed together in a furnace and subjected to prescribed

temperature excitations, typically in the form of a continuous ramp or a step-wise temperature change.

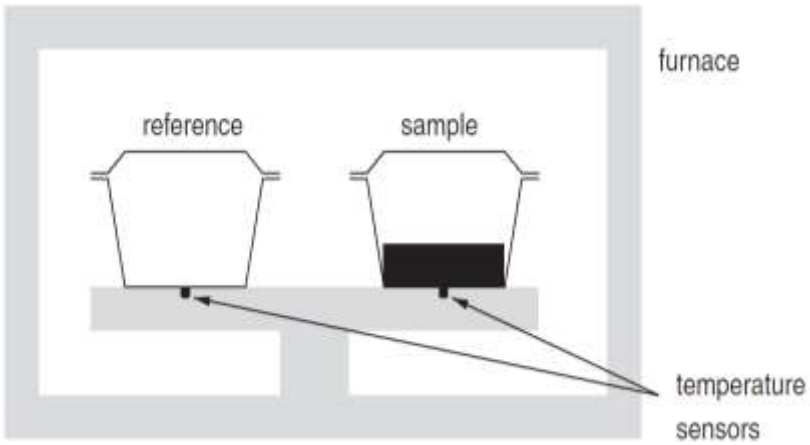

FIGURE 3 – Furnace of a Heat Flux DSC (Castellon, 2008)

The difference in the amount of heat required to increase the temperature of the sample and the reference is measured as a function of temperature. During a phase transition more heat will flow either to or from the sample compared to the reference, depending on whether the sample is solidifying or melting. The difference in the magnitude of heat flows in the sample and the reference lead to a voltage difference between the samples. From this voltage difference the actual quantity of absorbed or released heat from the sample can be determined. This measurement of the heat flow associated with the sample can be processed with commercial software resulting in the determination of the specific heat capacity and enthalpy as a function of temperature.

There are two operational methods, distinguished by their respective temperature profiles, which can be used to determine the enthalpy as a function of temperature of a PCM sample using heat flux DSC. They are the dynamic and isothermal step methods. The dynamic method is the most commonly used method; however, this method often results in values of the enthalpy as a function of temperature for the PCM that are incorrect. The dynamic method involves heating and cooling sections that are performed at constant temperature change rates. Rates between 1°C/min and 10°C/min are common. Figure 4 illustrates a heat flow curve for a dynamic cooling run at 1°C/min for a microencapsulated paraffin based PCM from Microtek Laboratories (Microtek, 2010). The measurement was performed with a TA Instruments Q20 DSC.

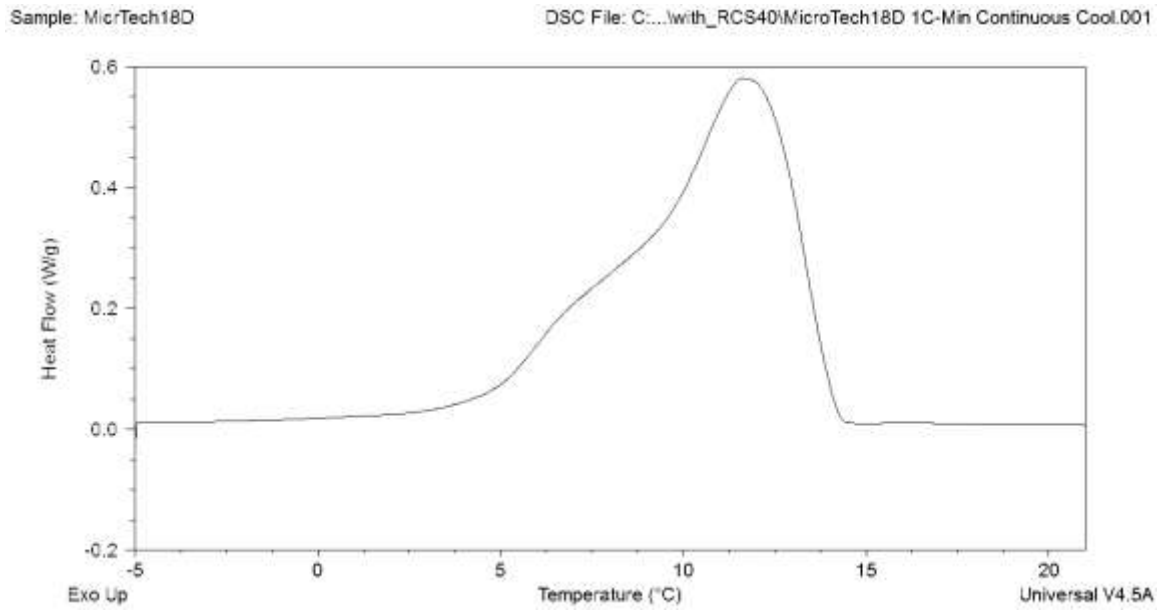

FIGURE 4 – Dynamic Method Profile of Microtek 18D Microencapsulated PCM

The heat flow values obtained from heating/cooling the PCM sample using the dynamic method are systematically shifted to higher/lower temperatures due to temperature gradients inside the PCM sample (Castellon et al., 2008). The temperature gradients are dependent on both the heating/cooling rate and the sample size. The shifting of the heat flow values results in inaccuracies in the enthalpy as a function of temperature values obtained through the post processing step. The temperature gradients within the sample leading to these inaccuracies are illustrated in Figure 5, where the solid lines represent the desired isothermal sample temperature and the dashed lines represent the actual sample temperature. It is clear that the heat flows into or out of the sample are not measured at a single temperature, but rather at a range of temperatures.

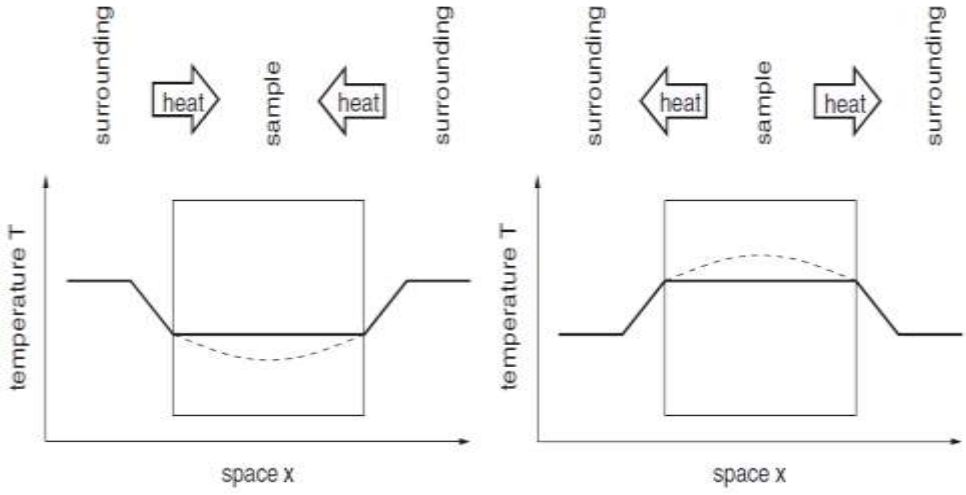

FIGURE 5 – Heating and Cooling Sample Temperature Distributions (Castellon, 2008)

The isothermal step method has been proposed in an effort to eliminate the errors associated with the thermal gradients throughout the PCM sample. This method is independent of sample size and heating/cooling rates (Castellon et al., 2008). In contrast to the dynamic method the isothermal step method does not incorporate continuous heating and cooling routines. Rather, the DSC furnace undergoes stepwise heating in given temperature intervals. At the beginning of a stepped temperature increase, the sample's heat flow signal deviates from the baseline, indicating that latent heat storage is occurring over that step interval. When the sample signal returns to the baseline during the same step interval it is known that the sample and its reference are isothermal; therefore, there is no temperature gradient in the sample. At this point the next step can follow. The area below the peak generated throughout the step is proportional to the heat absorbed by the sample during that step (Gunther et al., 2009). By integrating over each of the step intervals the enthalpy as a function of temperature is obtained. Figure 6 illustrates a heat flow curve for an isothermal step cooling routine at 0.5°C step intervals for a microencapsulated paraffin based PCM from Microtek Laboratories (Microtek, 2010). The measurement was performed with a TA Instruments Q20 DSC.

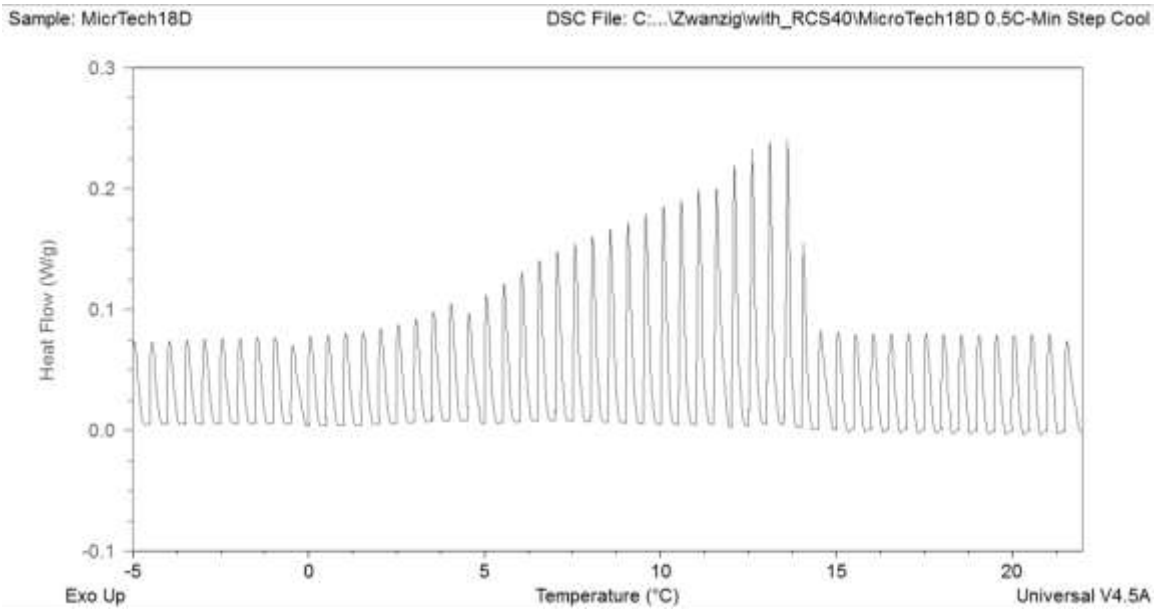

FIGURE 6 – Isothermal Step Method Cooling Profile of Microtek 18D Microencapsulated PCM

The integration of the peaks in Figure 6 leads to the enthalpy and phase fraction curves shown in Figure 7. The determination of the phase fraction curve from the enthalpy data is described in the following section.

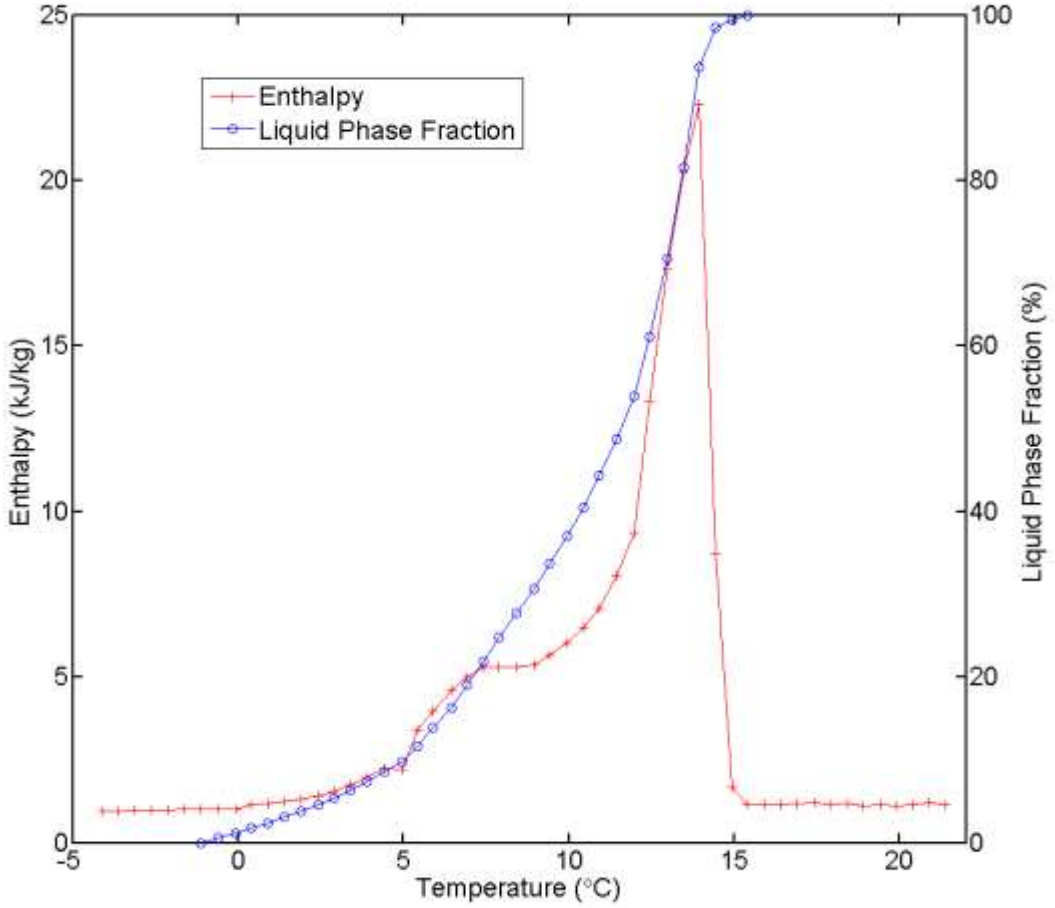

FIGURE 7 – Enthalpy and Phase Fraction Cooling Curves for MicroTek 18D

In general, physical property characterization with DSC suffers from the limitation that the sample size is only a few milligrams and therefore property information for PCM impregnated building materials may not be obtainable, depending on the characteristic size of the product in question. However, once the PCM properties are known, the properties of a PCM integrated building materials can be estimated based

on the mass or volume fraction of PCM to composite materials (Stovall & Tomlinson, 1995).

2. Modeling

Several authors (Castellon et al., 2008; Gunther et al., 2009; Fang and Madina, 2009) have performed measurements to verify that the isothermal step method provides the enthalpy as a function of temperature of a PCM sample independent of temperature rate of change and sample size. With such a precise measurement of the PCM's enthalpy as a function of temperature, it is possible to simulate the PCM performance in a building envelope accurately, without the danger of either over or underestimating the thermal storage capacity of the PCM enhanced building envelope in question.

Having determined a PCM's enthalpy as a function of temperature by the isothermal step method, it is possible to proceed with the modeling of that PCM using the assumption that the heat absorbed or released at a certain temperature during the phase transition is only a function of temperature (Fang and Madina, 2009). Fang and Madina (2009) showed through DSC measurement that, during the phase change process, the latent heat is not evenly absorbed and released along the phase change temperature range. Furthermore, PCMs in walls or roofs will typically not be operating under ideal conditions where the entire phase change transition occurs in every diurnal cycle. In fact, it is more common that the phase change process will begin from a partially melted state, resulting from incomplete nighttime solidification, partial day time melting, or

temperature fluctuations throughout the day (Fang and Madina, 2009). Representing the heat absorbed or released during the phase change process as a function of temperature allows the model to be applied to the phase change processes from either completely melted or partially melted states, accurately accounting for the energy storage and release in these scenarios.

Figure 8 displays enthalpy as a function of temperature of a paraffin PCM measured by DSC using the isothermal step method (Fang and Madina, 2009).

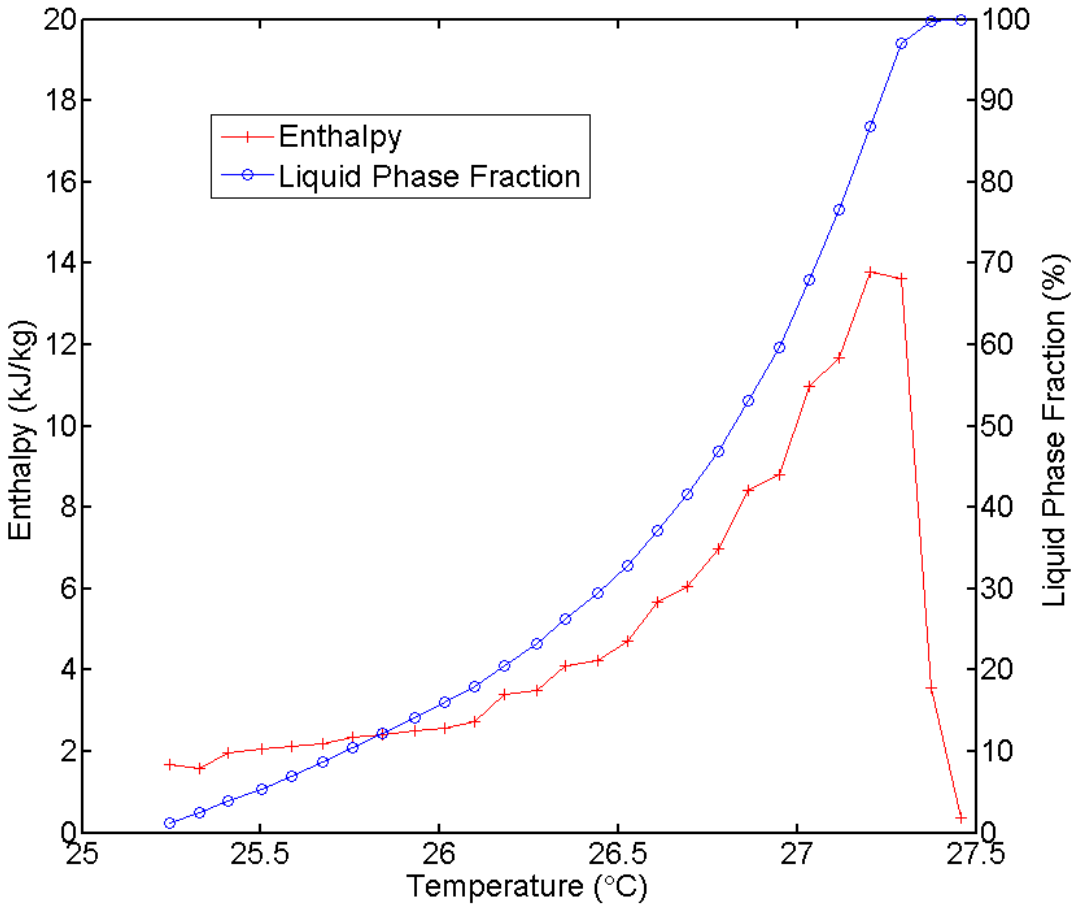

FIGURE 8 – Enthalpy and Phase Fraction Curves of PCM (Reproduced from Fang and Madina, 2009)

The data is incorporated into the model through a latent heat source term in the form of the phase fraction, $g_l(T)$, determined by

$$g_l(T) = \frac{\Delta H_T}{\Delta H} \tag{1}$$

where ΔH_T is the enthalpy released/absorbed at a given temperature and ΔH is the total enthalpy released or absorbed over the entire phase change temperature range. The

following assumptions are made using this model: (1) the heating and solidification enthalpy curves are symmetrical to one another and (2) for the partially melted phase change processes, with heating and solidification starting from different partially melted states, the enthalpy curves follow the same curves as the continuous phase transition process (Fang and Madina, 2009).

F. Scope of Work

Many studies have been conducted to understand the potential benefits of incorporating PCMs into building construction and, as shown in Figure 9, the number of journal articles that have been dedicated to this work has grown tremendously over the past 5 years. The intent of this work was to numerically investigate the impact that PCM composite materials have on annual load reduction, peak load reduction, and peak load shifting when implemented in residential buildings. Specifically, this study investigated the effects of the location of a PCM composite wallboard within multi-layered wall/roof systems in three climate zones. A single PCM was used in all simulations. The simulations were executed over an entire year using TMY3 (NREL, 2008) weather data gathered in Minneapolis, MN, Louisville, KY, and Miami, FL. In this way the effect on both heating and cooling loads can be analyzed so that the net effect of the PCM installation on annual energy use can be determined. The performance of the PCM enhanced building envelopes were quantified by determining annual load reduction, peak load reduction, and peak load shifting potential.

Additional effects that were considered included the performance of the PCM in three varied climate zones and, for each climate zone, the optimal location of the PCM within the multi-layered building envelope was determined.

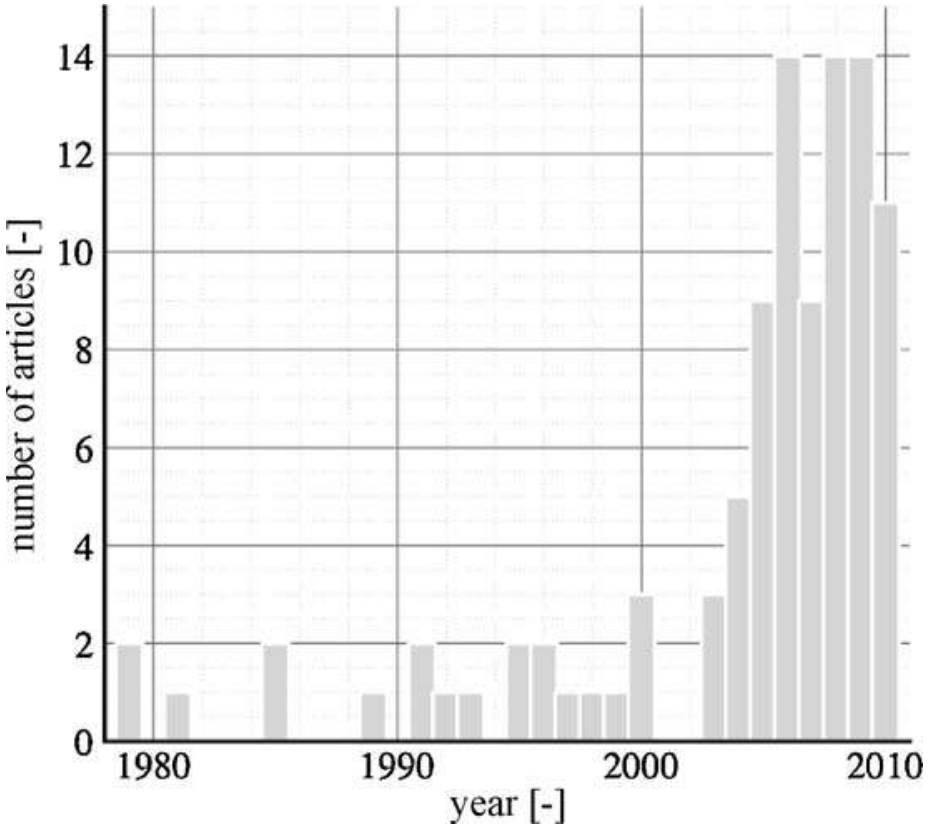

FIGURE 9 – Number of Publications Concerning PCMs in Building Envelopes Since 1979 (Kuznik, 2011)

The thesis covers the following topics: development of the numerical model and boundary conditions used in the study, the validation of the numerical model against

analytical solutions of simplified systems found in the literature, a description of the multi-layered wall/roof systems being simulated, a presentation of the results and interesting findings, and finally the conclusion and recommendations for future work.

II. MODEL DEVELOPMENT

A. Governing Equation

The heat transfer through the multi-layered wall/roof systems is described by the one-dimensional transient heat conduction equation originally used in the STAR (Simplified Transient Analysis of Roofs) program (Wilkes, 1989). (The program was written using Fortran 77. To make it more structured, the program was rewritten using Fortran 90.) The program solves the following one-dimensional equation

$$c_p \rho \frac{\partial T}{\partial t} = \frac{\partial}{\partial x}\left(k \frac{\partial T}{\partial x}\right) \tag{1}$$

where c_p is the heat capacity, ρ is the material density, T is the temperature, and k is the conductivity. For multi-layered wall systems, the contact resistance between different layers is not considered. To account for the latent heat effect, a PCM model is incorporated into the program. Following the work of Voller and Swaminathan (1990), the PCM model is represented by a non-linear source term in the governing equation. With PCM the heat transfer equation is written as follows:

$$c_p \rho \frac{\partial T}{\partial t} = \frac{\partial}{\partial x}\left(k \frac{\partial T}{\partial x}\right) - L \rho_{pcm} \frac{\partial g_l}{\partial t} \tag{2}$$

where L is the latent heat of the PCM, ρ_{pcm} is the density of the PCM, and g_l is the liquid phase fraction. The phase change transition occurs over a temperature range and the phase fraction is an invertible function of temperature where

$$g_l = F(T) \tag{3a}$$

$$0 \leq g_l \leq 1 \tag{3b}$$

$$g_l = \begin{cases} 1 \; liquid \\ 0 \; solid \end{cases} \tag{3c}$$

Here the function F represents the curve generated by eq. 1 shown in Figure 8. For a composite PCM wallboard, the material properties c_p and ρ are mass fraction averaged properties defined as follows:

$$\rho_c = \left(1 - \mathrm{W_{pcm}}\right)\rho_{\mathrm{gyp}} + \mathrm{W_{pcm}}\left(\rho_{\mathrm{pcm,l}}\mathrm{g_l} + \rho_{\mathrm{pcm,s}}(1 - \mathrm{g_l})\right) \tag{4}$$

$$c_{p,c} = \left(1 - \mathrm{W_{pcm}}\right)\mathrm{c_{p,gyp}} + \mathrm{W_{pcm}}\left(\mathrm{c_{p,pcm,l}}\mathrm{g_l} + \mathrm{c_{p,pcm,s}}(1 - \mathrm{g_l})\right) \tag{5}$$

where W_{pcm} is the mass fraction of the PCM in the composite, $c_{p,gyp}$, $c_{p,pcm,l}$, $c_{p,pcm,s}$ are the specific heat of gypsum, liquid phase PCM, and solid phase PCM respectively and ρ_{gyp}, $\rho_{pcm,l}$, and $\rho_{pcm,s}$ are the density of gypsum, liquid phase PCM and solid phase PCM respectively. The thermal conductivity of the composite PCM wallboard is determined using Maxwell's derivation for inclusions in a continuous solid phase (Bird et al., 2007)

$$k_c = k_{gyp}\left(1 + \frac{3\varphi}{\left(\frac{k_{pcm}+2k_{gyp}}{k_{pcm}-k_{gyp}}\right)-\varphi}\right) \tag{6}$$

where k_{pcm} and k_{gyp} are the thermal conductivities of PCM and gypsum, and the volume fraction , φ, is given as

$$\varphi = W_{pcm}\frac{\rho}{\rho_{pcm}} \tag{7}$$

The phase fraction g_l is known at simulation time $\tau = 0$ facilitating the initialization of all material properties.

B. Boundary Conditions

Proper boundary conditions are required to solve Eqs. (1) and (2). Figure 10 depicts the boundary conditions incorporated into the model. The exterior surfaces are subject to excitations from both convection and radiation heat transfer with the ambient air and surroundings. The radiation is from air, ground and sky.

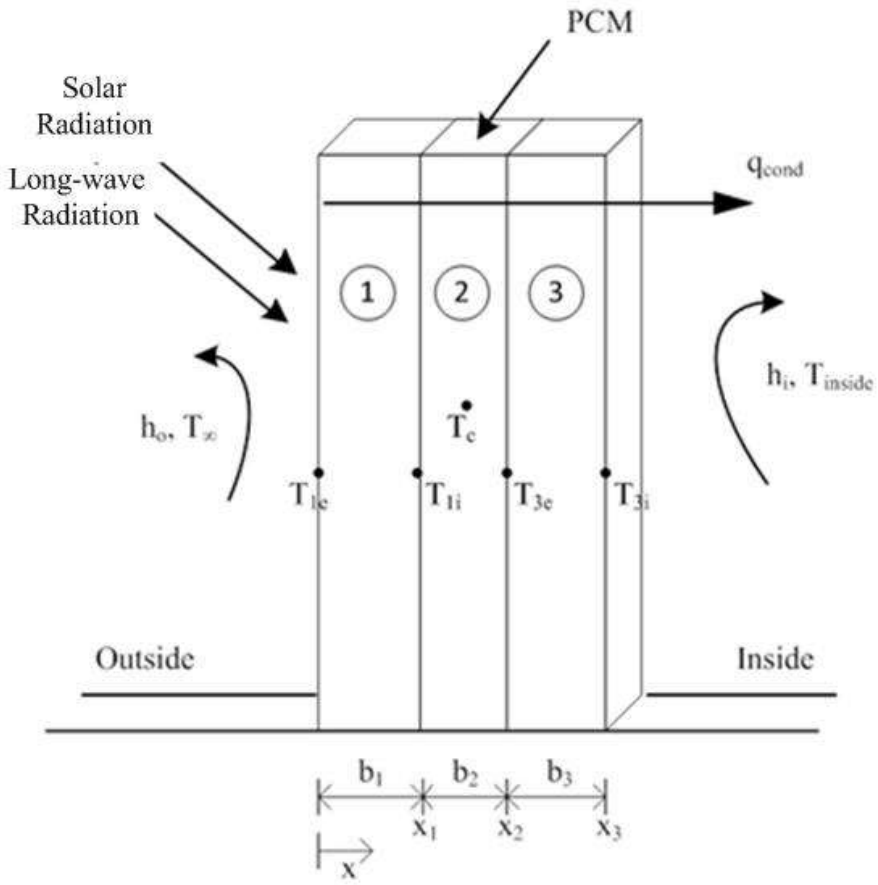

FIGURE 10 – A Demonstration Multi-layered PCM Enhanced Wall with Boundary Conditions

Referring to Figure 10, at the exterior boundary condition of $x = x_0$ the following Neumann boundary condition is applied,

$$-k\frac{\partial T}{\partial x}\Big|_{x_0} = h_{r,sky}\left(T_{sky} - T_{1e}\right) + h_{r,air}(T_{air} - T_{1e}) + h_{r,gnd}\left(T_{gnd} - T_{1e}\right) + \alpha Q_{sun} + h_o(T_{air} - T_{1e}) \quad (8)$$

where the $h_{r,sky}$, $h_{r,air}$, and $h_{r,gnd}$ are radiation heat transfer coefficients from sky, air and ground respectively and are linearized as

$$h_{r,sky} = \varepsilon\sigma F_{sky}\beta\left(T_{sky}^2 + T_{1e}^2\right)\left(T_{sky} + T_{1e}\right) \quad (9)$$

$$h_{r,air} = \varepsilon\sigma F_{sky}(1-\beta)(T_{air}^2 + T_{1e}^2)(T_{air} + T_{1e}) \quad (10)$$

$$h_{r,gnd} = \varepsilon\sigma F_{gnd}\left(T_{gnd}^2 + T_{1e}^2\right)\left(T_{gnd} + T_{1e}\right) \quad (11)$$

here α, ε, σ, F, and β as absorptivity, emissivity, Stefan-Boltzmann constant, view factor, and the air-sky attenuation factor respectively. The calculation of the value for Q_{sun} that

is input into Eq. (8) is explained in the following section. In Eq. (8) h_o is the mixed convection heat transfer coefficient that is found using the correlation given by Incropera et al. (2007). In order to calculate the mixed convection coefficient it is necessary to first calculate the forced and natural convection coefficients. The correlations used for isothermal flat plates for forced convection are found in Holman (1981). The correlations used for isothermal flat plates under natural convection with horizontal, near horizontal (up to 2 degrees of tilt), vertical, and tilted (greater than 2 degrees of tilt) orientations are also found in Holman (1981). In Eq. (9) the sky temperature, T_{sky}, is determined as follows (EnergyPlus, 2010). First, the emissivity of the sky is calculated

$$\varepsilon_{sky} = \left[0.787 + 0.764 \log\left(\frac{T_{dewp}+273.15}{273}\right)\right](1 + 0.0224C_{amt} + 0.0035C_{amt}^2 + 0.00028C_{amt}^3) \quad (12)$$

where T_{dewp} is the dewpoint temperature and C_{amt} is the cloud amount, taken from TMY3 data files. Next, the infrared radiation emitted from the sky is calculated by

$$I_{IR} = \varepsilon_{sky}\sigma T_{drybulb}^4 \quad (13)$$

where $T_{drybulb}$ is taken as the ambient air temperature from TMY3 data files. Finally, the sky temperature is found to be

$$T_{sky} = \left(\frac{I_{IR}}{\sigma}\right)^{0.25} \tag{14}$$

Special treatment is needed at the interface between a PCM wallboard and a non-PCM wallboard. For instance, in Figure 10, layer 1 is a non-PCM wallboard and layer 2 is a PCM wallboard. If the PCM composite layer 2 is not undergoing a phase transition then the following energy balance is applied at interface x_1

$$-k\frac{\partial T}{\partial x}\Big|_{x_{1,layer\ 1}} = -k\frac{\partial T}{\partial x}\Big|_{x_{1,layer\ 2}} \tag{12}$$

When a phase transition occurs, the energy balance becomes

$$-k\frac{\partial T_1}{\partial x}\Big|_{x_1,layer\ 1} = L\rho_{pcm}\frac{\partial g_l}{\partial t} - k\frac{\partial T}{\partial x}\Big|_{x_{1,layer\ 2}} \tag{13}$$

The interior surface at $x=x_3$ is subject to both convective and radiative heat transfer and the following boundary condition is applied,

$$-k\frac{\partial T}{\partial x}\Big|_{x_3} = h_{r,i}(T_i - T_{3i}) + h_i(T_i - T_{3i}) \quad (14)$$

where h_i is found using the correlations for isothermal flat plates discussed above and $h_{r,i}$ is the linearized radiative heat transfer coefficient. The room temperature, T_i, varies between seasons and is 20°C for the heating season and 24°C for the cooling season. The heating season is defined as the months that require heating for the majority of the days. Likewise the cooling season is defined as the months that require cooling for the majority of the days.

C. Anisotropic Sky Model

The solar radiation data for fulfilling the outer boundary condition is generated with the anisotropic sky model of Hay, Davies, Klucher, and Reindl (HDKR) using TMY3 (Typical Meteorological Year 3) data from collection stations in Minneapolis, MN, Louisville, KY, and Miami, FL as inputs. The HDKR model presented by Duffie and Beckman (1991) allows boundary conditions to be generated for all building surfaces

with any directional orientation and tilt. This model accounts for beam, circumsolar diffuse, isotropic diffuse, horizon-brightening, and ground reflected radiation.

The total radiation on a tilted surface is given by

$$I_T = (I_b + I_d A_i) R_b + I_d (1 - A_i) \left(\frac{1+\cos\beta}{2}\right) \left[1 + f \sin^3\left(\frac{\beta}{2}\right)\right] + I \rho_g \left(\frac{1-\cos\beta}{2}\right) \quad (15)$$

where I_b is beam radiation incident on a horizontal surface, I_d is diffuse radiation incident on a horizontal surface, A_i is the anisotropy index, R_b is the beam ratio, β is the tilt angle of the surface from horizontal, f is the modulating factor, I is the total radiation on a horizontal surface, and ρ_g is the ground reflectance. The values for the total radiation on a horizontal surface, I, and the diffuse radiation on a horizontal surface, I_d, are taken from TMY3 data files. The beam radiation is calculated as

$$I_b = I - I_d \quad (16)$$

The anisotropy index is a function of the transmittance of the atmosphere and determines the forward scattered portion of the horizontal diffuse radiation. It is determined by

$$A_i = \frac{I_b}{I_o} \tag{17}$$

where I_o is the radiation incident on a horizontal surface outside of the atmosphere and is found by

$$I_o = \frac{12 \times 3600}{\pi} G_{sc} \left(1 + 0.033 \cos \frac{360n}{365}\right) \times \left[\cos\varphi \cos\delta \left(\sin\omega_2 - \sin\omega_1\right) + \frac{\pi(\omega_2 - \omega_1)}{180} \sin\varphi \sin\delta\right] \tag{18}$$

where G_{sc} is the solar constant, n is the day of the year, ϕ is the latitude of the location, δ is the declination angle, and ω is the hour angle. The declination angle, δ, is given by

$$\delta = 23.45 \sin\left(360 \times \frac{284+n}{365}\right) \tag{19}$$

where n is once again the day of the year. The hour angle, ω, is found by first calculating the equation of time given by

$$E = 229.2(0.000075 + 0.001868\cos B - 0.032077\sin B - 0.014615\cos 2B - 0.04089\sin 2B) \quad (20)$$

where B is found, with n being the day of the year, by

$$B = (n-1)\frac{360}{365} \quad (21)$$

Next, the solar time is calculated by

$$Solar\ time = standard\ time + 4(L_{st} - L_{loc}) + E \quad (22)$$

where L_{st} is the standard meridian for the local time zone and L_{loc} is the longitude of the location in degrees west, i.e. $0° < L_{loc} < 360°$, and E is the equation of time. Finally ω can be determined as

$$\omega = (solar\ time - 12) \times 15° \quad (23)$$

The beam ratio, R_b, must now be calculated. This is a geometric factor represented by the ratio of beam radiation on a tilted surface to that on a horizontal surface and facilitates the determination of the incident radiation on a tilted surface. R_b is found using the following equation

$$R_b = \frac{\cos\theta}{\cos\theta_z} \tag{24}$$

where θ is the angle of incidence between the surface in question and the beam radiation and θ_z is the zenith angle or the angle of incidence of beam radiation and on a horizontal surface. The angle of incidence of the surface in question, θ, is calculated as follows

$$\cos\theta = \sin\delta\sin\varphi\cos\beta - \sin\delta\cos\varphi\sin\beta\cos\gamma + \cos\delta\cos\varphi\cos\beta\cos\omega + \cos\delta\sin\varphi\sin\beta\cos\gamma\cos\omega + \cos\delta\sin\beta\sin\gamma\sin\omega \tag{25}$$

where γ is the surface azimuth angle. The zenith angle, θ_z, can be found using Eq. 25 and setting the surface tilt angle, β, equal to zero. The following equation results

$$\cos\theta_z = \cos\varphi\cos\delta\cos\omega + \sin\varphi\sin\delta \tag{26}$$

The last remaining term to be defined in order to evaluate the HDKR model is the modulating factor, *f*, which is a correction factor for the horizon brightening term and is determined by

$$f = \sqrt{\frac{I_b}{I}} \tag{27}$$

Finally, in order to ensure that the generated values of incident solar radiation on the walls of the building is accurate, the self-shading of the building must be taken into consideration. This necessitates the calculation of the solar azimuth angle which is given as

$$\gamma_s = \text{sign}(\omega) \left| \cos^{-1} \left(\frac{\cos\theta_z \sin\varphi - \sin\delta}{\sin\theta_z \cos\varphi} \right) \right| \tag{28}$$

where the sign( ) function is equal to +1 if ω is positive and -1 if ω is negative. Now, if the quantity $|\gamma - \gamma_s|$ is greater than 90° and less than 270° then the solar radiation on the wall in question is due to the isotropic diffuse components alone. The HDKR model has

been implemented in a boundary condition generating program written with FORTRAN 90.

D. Numerical Procedure

A finite volume scheme is used to solve the one-dimensional transient heat conduction equation (2). A sample computational grid is shown in Figure 11: a representative finite volume is marked with red.

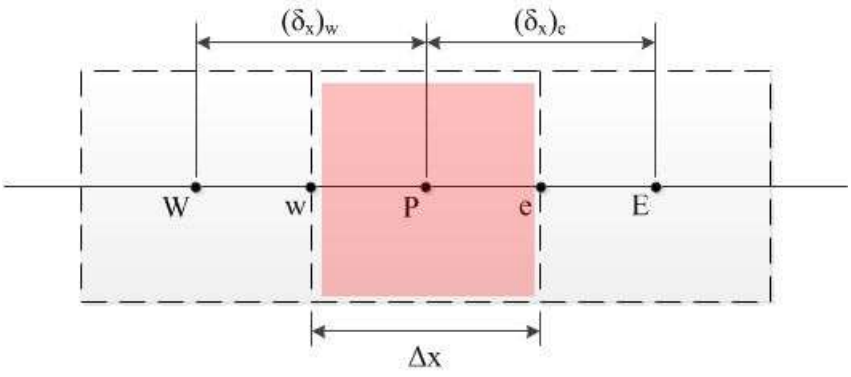

FIGURE 11 – One-Dimensional Finite Volume Grid

The left and right boundaries of the finite volume are marked as w and e, respectively. If we integrate the conductivity term over the control volume we have

$$\int_{CV} \frac{\partial}{\partial x}\left(k\frac{\partial T}{\partial x}\right) dV = \left(k_e A_f \frac{\partial T}{\partial x}\right)_e - \left(k_w A_f \frac{\partial T}{\partial x}\right)_w \tag{15}$$

where k_w and k_e are the conductivities at the left and right interfaces of the control volume and A_f is the face area of the control volume. In the numerical analysis, only properties on the control volume center are defined and the values on the interfaces are obtained through interpolation. To this end, at material interfaces the following effective thermal conductivity proposed by Patankar (1980) is used

$$k_e = \left(\frac{1-f_e}{k_P} + \frac{f_e}{k_E}\right)^{-1} \tag{16}$$

where k_P and k_E are the thermal conductivities of the control volumes containing points P and E respectively and f_e is defined as

$$f_e = \frac{(\delta_x)_{e+}}{(\delta_x)_e} \tag{17}$$

where $(\delta_x)_{e+}$, from Eq. (17), and $(\delta_x)_{e-}$, shown in Figure 12, denote the distances between the interface and the neighboring nodes and $(\delta_x)_e$ is the total distance between the neighboring nodes, also shown in Figure 12.

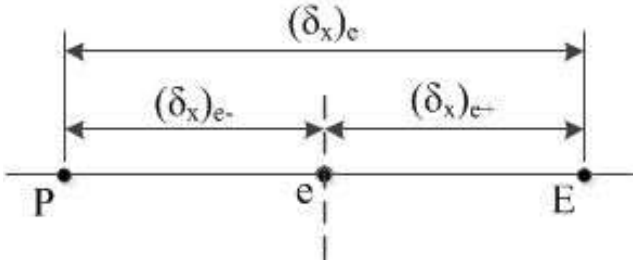

FIGURE 12 – Node Spacing for Definition of Effective Thermal Conductivity

The central difference scheme is used to discretize the first order derivative as follows:

$$\left(\frac{\partial T}{\partial x}\right)_e = \frac{T_E - T_P}{(\delta_x)_e} \tag{18}$$

Applying the Crank-Nicolson scheme to the governing equation leads to the following

$$\rho c_p \frac{\Delta x}{\Delta t}(T_P^n - T_P^{n-1}) = f\left[\frac{k_e}{(\delta_x)_e}(T_E^n - T_P^n) - \frac{k_w}{(\delta_x)_w}(T_P^n - T_W^n)\right] + (1-f)\left[\frac{k_e}{(\delta_x)_e}(T_E^{n-1} - T_P^{n-1}) - \frac{k_w}{(\delta_x)_w}(T_P^{n-1} - T_W^{n-1})\right] - \rho_{pcm} L \frac{\Delta x}{\Delta t}(g_l^n - g_l^{n-1}) \tag{19}$$

where superscript *n* is the current time step, subscripts *P*, *E*, and *W* are the nodal locations and *f* is a weighting factor which is defined as $f = 0.5$. From Eq. (3a) it is known that g_l is a nonlinear function of temperature, hence Eq. (19) is a nonlinear equation for the temperature and can be solved using an iterative method discussed by Kousksou et al. (2006). At the beginning of each time step, the unknown g_l^n is calculated based on the temperature from the previous time step, t^{n-1}. An intermediate temperature T^{m+1} is calculated by solving the system of equations (19). The calculated temperature T^{m+1} is then used to update the unknown g_l. This iterative process repeats until a converged solution is reached. The iterative method can be expressed mathematically as follows:

$$\rho c_p \frac{\Delta x}{\Delta \mathrm{t}}(T_P^{m+1} - T_P^{n-1}) = f\left[\frac{k_e}{(\delta_x)_e}(T_E^{m+1} - T_P^{m+1}) - \frac{k_w}{(\delta_x)_w}(T_P^{m+1} - T_W^{m+1})\right] +$$

$$(1-f)\left[\frac{k_e}{(\delta_x)_e}(T_E^{n-1} - T_P^{n-1}) - \frac{k_w}{(\delta_x)_w}(T_P^{n-1} - T_W^{n-1})\right] - \rho_{pcm} L \frac{\Delta \mathrm{x}}{\Delta t}(g_l^{m+1} - g_l^{n-1}),$$

$$\mathrm{m}=1,2,\ldots \qquad (20)$$

At the (m+1)-th iteration the liquid phase fraction g_l^{m+1} is linearized from the previous m-th iteration by

$$g_l^{m+1} = g_l^m + \left.\frac{dg_l}{dT}\right|_{T=T_P^m}(T_P^{m+1} - T_P^m) \qquad (21)$$

Substituting Eq. (21) into Eq. (20) a linear system of equations of T^{m+1} is obtained

$$\left[a_P + \rho_{pcm} L \frac{\Delta x}{\Delta t} \frac{dg_l}{dT}\right] T_P^{m+1} + a_W T_W^{m+1} + a_E T_E^{m+1} = \left[b^{n-1} - \rho_{pcm} L \frac{\Delta x}{\Delta t}\left(g_l^m - g_l^{n-1} - \frac{dg_l}{dT} T_P^m\right)\right] \quad (22)$$

where

$$a_W = -f \frac{k_w}{(\delta_x)_w} \quad (23)$$

$$a_E = -f \frac{k_e}{(\delta_x)_e} \quad (24)$$

$$a_P = \rho c_p \frac{\Delta x}{\Delta t} - a_W - a_E \quad (25)$$

$$b^{n-1} = (1-f)\left[\frac{k_e}{(\delta_x)_e}(T_E^{n-1} - T_P^{n-1}) - \frac{k_w}{(\delta_x)_w}(T_P^{n-1} - T_W^{n-1})\right] + \rho c_p \frac{\Delta x}{\Delta t} T_P^{n-1} \quad (26)$$

Equation 22 is a set of algebraic equations that can be solved iteratively employing the well known tri-diagonal matrix algorithm (TDMA) (Patankar, 1980). Rewrite Eq. 22 in the following compact form

$$A_i T_{i-1} + B_i T_i + C_i T_{i+1} = D_i,\ i = 1..n \tag{27}$$

with A_1=0 and C_n=0 the linear system of equations is solved in two steps. First a forward sweeping step to modify the coefficients where

$$C_i^{'} = \begin{cases} \frac{C_i}{B_i},\ i = 1 \\ \frac{C_i}{B_i - C_{i-1}^{'} A_i},\ i = 2,3,\dots,n-1 \end{cases} \tag{28}$$

and

$$D_i^{'} = \begin{cases} \frac{D_i}{B_i},\ i = 1 \\ \frac{D_i - D_{i-1}^{'} A_i}{B_i - C_{i-1}^{'} A_i},\ i = 2,3,\dots,n \end{cases} \tag{29}$$

Then the solution is obtained through a back substitution process by

$$T_n = D_n^{'} \tag{30}$$

$$T_i = D_i^{'} - C_i^{'} T_{i+1};\ \ i = n-1, n-2, \ldots, 1 \tag{31}$$

This solution process is repeated until the convergence criterion given in Eq. 32 is met.

$$\varepsilon \leq 10^{-5} \tag{32}$$

III. MODEL VERIFICATION

The numerical model described previously was verified by comparing simulation results to analytical solutions. In the first test heat conduction through a plane wall with finite thickness and infinite width and length is considered. The wall is subjected to convection on the top and bottom surfaces. The problem can be simplified as a one-dimensional heat conduction problem and an analytical solution exists (Nellis and Klein, 2009). The wall is 0.2 m thick and the Biot ($Bi=hx/k$) number is 10, where h, x, and k are the convection coefficient, location in the wall, and thermal conductivity respectively. The initial wall temperature is 20°C and the ambient temperature is 80°C. Figure 13 compares the numerical results with the analytical solutions at different Fourier numbers ($Fo=\alpha t/x^2$), where α, t, and x are the thermal diffusivity, time, and location in the wall respectively. Good agreement is shown. The temperature profiles at different Fourier numbers are displayed with the mid-plane labeled as x = 0 m.

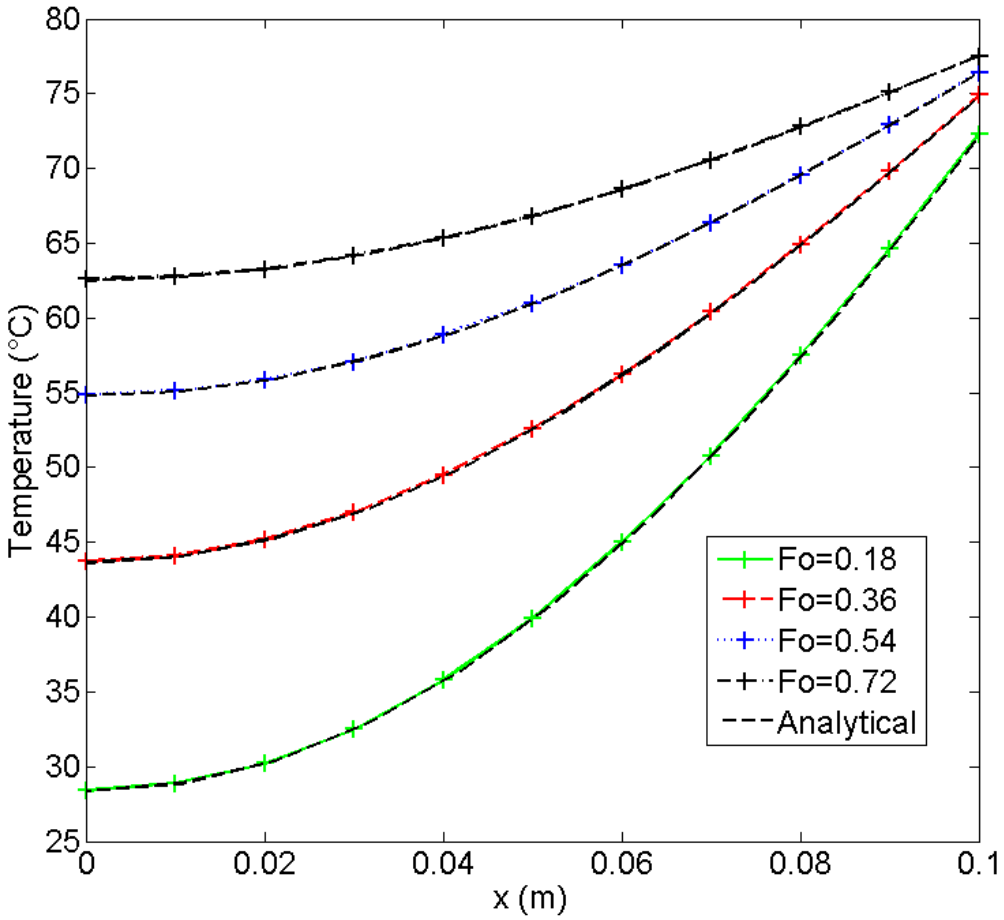

FIGURE 13 – Plane Wall with Convection, Analytical vs. Numerical with Fo = 0.18, 0.36, 0.54, 0.72

In the second test, the two-phase Stefan problem developed by Solomon (1979) is studied. The geometry is a semi-infinite PCM slab initially at a constant temperature of 21°C and in the solid phase throughout. A constant temperature boundary condition of 95°C is enforced on the top and the PCM slab is adiabatic on the sides and bottom, as shown in Figure 14. Solomon (1979) shows that the semi-infinite slab approximation

developed is applicable to a finite slab case for t ≤ 7891 s given a length of 0.1m in the direction of interest.

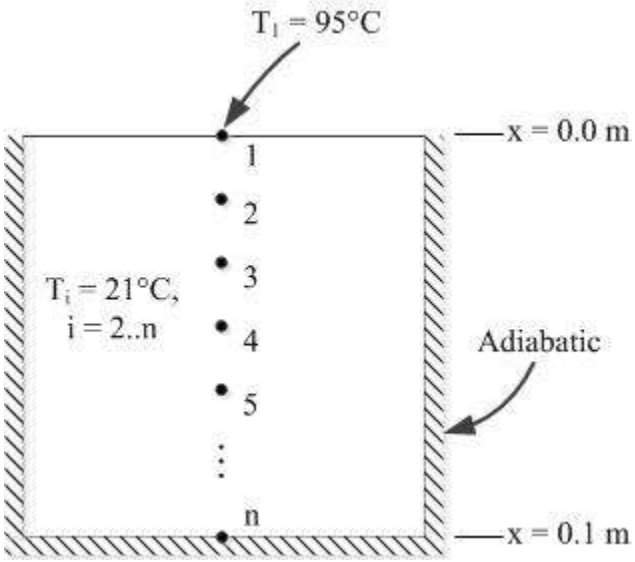

FIGURE 14 – Two-phase Stefan Problem Geometry with Boundary Conditions

The analytical solution presented by Solomon (1979) exists when an isothermal phase change is assumed, i.e. the phase transition occurs at a single temperature, given as T_m. Because the model developed in this work does not simulate an isothermal phase transition, but rather utilizes the liquid phase fraction described previously, it is necessary to choose a phase transition temperature range, resulting in minor disagreement between the temperature profiles of the analytical and numerical solutions. As expected and as

shown in Figure 15, the narrower the transition temperature range chosen the more closely the model matches the analytical solution.

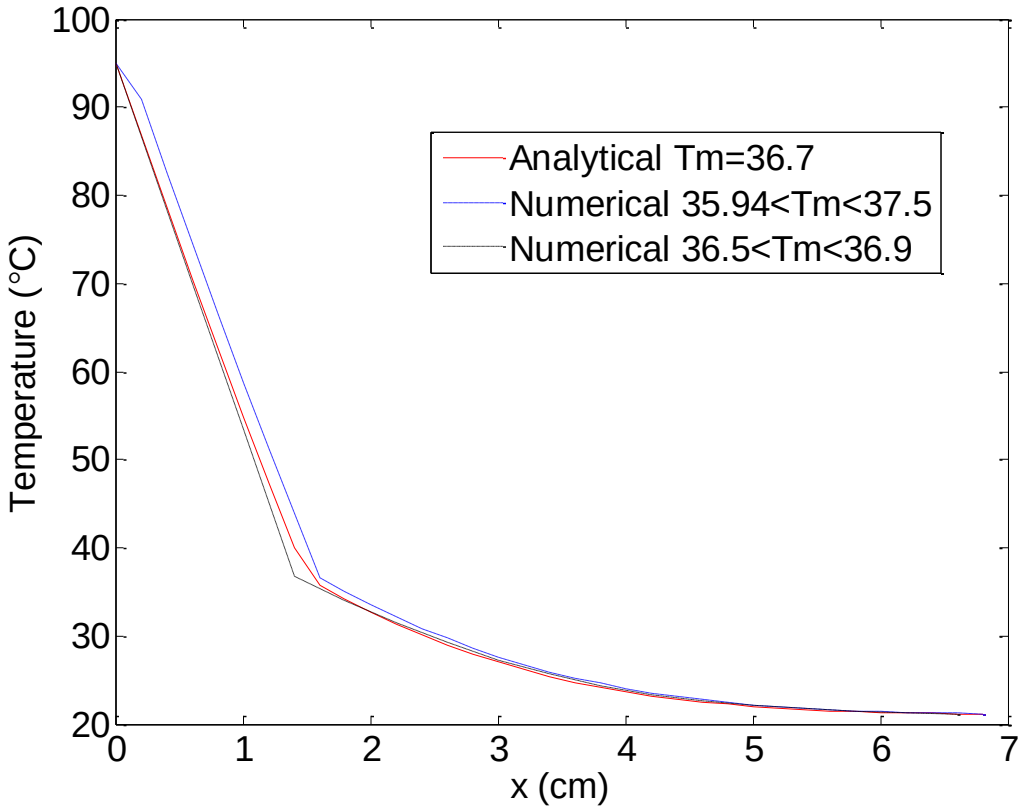

FIGURE 15 – Two-phase Stefan Problem, Analytical vs. Numerical

Next, the energy transferred to the system in the simulation of the two-phase Stefan problem was verified against the analytical solution. The analytical solution predicts that the energy stored in the system as both latent and sensible heat is 4446 kJ/m^2 at t = 3600 s. Table II shows that the accuracy of the energy balance is dependent on the selection of time step with better matching at the higher temporal resolution (small Δt).

TABLE II

TOTAL HEAT ENERGY STORED (AT t = 3600 s) AS A FUNCTION OF Δt FOR THE TWO-PHASE STEFAN PROBLEM

Δt (s)	Total Stored Heat Predicted by the Model (kJ/m^2)	% Difference
2	3788.20	-14.8
1	4445.74	-0.0059

At Δt = 1 second the error in the simulated quantity of heat transferred to the system is -0.0059% when compared to the analytical solution.

Finally, it was verified that the temporal resolution of Δt = 1 second was high enough to provide accurate results when the simulation incorporated the phase fraction model shown in Figure 8. An energy balance was conducted on a simulation using this phase fraction model. A constant heat flux of 315.45 W/m^2 (100 $Btu/hr\text{-}ft^2$) was applied at the surface of a semi-infinite solid. Table III displays the results at one-hour intervals over four hours of simulated time. The good agreement between the energy put into the system and the actual energy stored in the system verifies that at Δt = 1 second, sufficient temporal resolution for the time dependent source term was achieved. This results in an accurate simulation result for the material model used.

TABLE III

TOTAL ENERGY STORED IN THE SYSTEM WITH CONSTANT FLUX

BOUNDARY CONDITION OF $q = 315.45\ W/m^2$ AND $\Delta t = 1\ s$

Time (hr)	Q (kJ/m^2)	% error
1	1153.94	-1.61
2	2269.37	0.085
3	3409.57	-0.077
4	4538.07	0.10

IV. SYSTEM DESCRIPTION

In this work a numerical study was performed to identify the performance of a PCM wallboard in building applications. More specifically a PCM composite wallboard incorporated into the walls and roof of a typical residential building located in three US climate zones, i.e. zones 1, 3, and 5, is examined. Cities representative of climate zones 1, 3 and 5 correspond to Minneapolis, MN, Louisville, KY, and Miami, FL respectively (EIA, 1996). The PCM performance was studied under all seasonal conditions and in three in-wall locations, described later as cases 1, 2, and 3. The primary objective was to show that PCM composite performance within the building envelope is highly dependent on the in-wall location chosen as well the climate in which the installation is located.

The multi-layered wall and roof assemblies were taken from ASHRAE Fundamentals (2001). Table IV provides the material properties of the wall and roof systems used in this study. The corresponding R-values for the walls and roof are 2.93 and 2.27 m^2K/W respectively.

TABLE IV

MATERIAL PROPERTIES OF MULTI-LAYERED WALL/ROOF (ASHRAE, 2001)

Layer #	Name	thickness (mm)	k (W/m-K)	ρ (kg/m^3)	c_p (kJ/kg-K)
Wall					
1	EIFS finish	9.5	0.72	1856	0.84
2	Insulation board	25.4	0.03	43	1.21
3	Fiberboard sheathing	12.7	0.07	400	1.3
4	Batt Insulation	89.4	0.05	19	0.96
5	Gypsum Board	15.9	0.16	800	1.09
Roof					
1	Built-up Roofing	9.5	0.16	1120	1.46
2	Fiberboard Sheathing	12.7	0.07	400	1.3
3	Insulation Board	50.8	0.03	43	1.21
4	Wood	50.8	0.15	608	1.63

The potential energy savings from the addition of a composite PCM wallboard will be determined for three different placement scenarios within the multi-layered roof and wall assemblies. For each of the walls, the PCM composite locations in the multi-layered assemblies are labeled cases 1 to 3 as shown in Figure 16. Case 1 has the PCM composite located between layers 1 and 2, case 2 has the PCM composite located between layers 3 and 4, and case 3 has the PCM composite replacing layer 5. For the roof, the PCM composite locations are also labeled as cases 1 to 3 as shown in Figure 17. Case 1 has the PCM composite between layers 1 and 2, case 2 has the PCM composite between layers 2 and 3, and finally case 3 has the PCM composite between layer 4 and the interior of the room. The PCM composite wallboard thickness used is 0.0127m (0.5 in.) which is typical of residential construction.

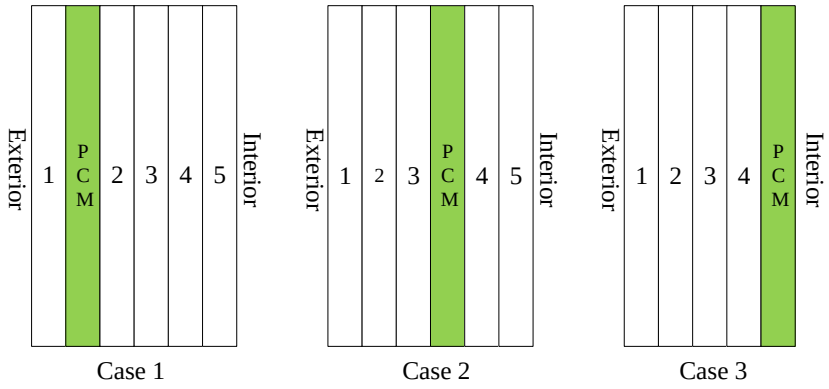

FIGURE 26 – Wall System PCM Composite Locations According to Case Number

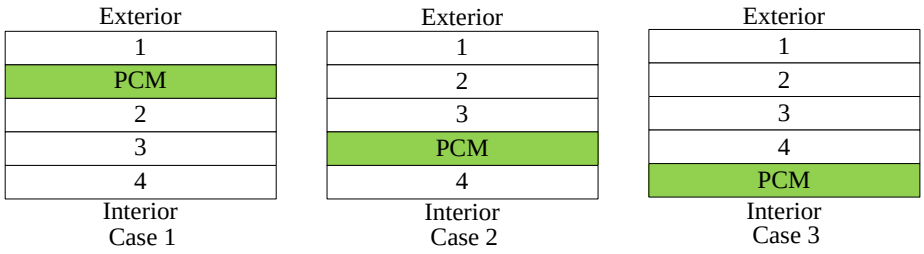

FIGURE 17 – Roof System PCM Composite Locations According to Case Number

The thermo-physical properties of the PCM composite wallboard containing a paraffin PCM (Fang and Madina, 2009) are shown in Table V. The volume fraction, φ, of PCM to gypsum is 25%. This is a volume fraction consistent with previously published values (Diaconu and Cruceru, 2010; Stovall and Tomlinson, 1995; Atheinitis et al, 1997). The phase fraction described in Section I-E-2 and shown in Figure 8 is applied to the model.

TABLE V

PCM COMPOSITE WALLBOARD MATERIAL PROPERTIES (φ=0.25)

PCM Wallboard Properties		
	Liquid	Solid
thickness (mm)	12.7	
k (W/m-K)	0.17	
c_p (kJ/kg-K)	1.46	1.29
ρ (kg/m^3)	790	829
L (kJ/kg)	33.5	

The building considered faces south with dimensions of 10.67m x 10.67m x 2.54m. All walls have dimensions of 10.67m x 2.54m and the flat roof is 10.67m x 10.67m. In the study windows and doors were not considered. The interior room temperature was considered to be uniform and heat transfer through walls and roof was assumed to be one-dimensional.

Since windows and doors were not considered in the simulations, the effects of solar heat gains/losses through windows and doors are neglected. Baseline simulations are run without PCM wallboard. Additional simulations were run with PCM wallboard without latent heat effect (assuming no phase change in the material) in order to distinguish between the effects of sensible and latent heat storage in the PCM composite wallboard. Finally, the simulations were initialized by repeating the first week of boundary conditions at the start of the simulation.

V. SIMULATION RESULTS

A. Simulation Description

The goal of this work was to study the effect of the addition of PCM composite wallboard in all four walls and the roof of the test building described in the previous section. The building performance was simulated using the exterior boundary conditions generated from TMY3 data for three U.S. climate zones. The climate zones simulated were 1, 3, and 5, represented by TMY3 data for Minneapolis, MN, Louisville, KY, and Miami, FL respectively. The PCM wallboard performance was quantified at three separate locations, the exterior, middle, and interior of the five multi-layered building envelope surfaces as shown in Figures 16 and 17, and labeled as cases 1, 2, and 3 respectively.

The performance of the PCM composite wallboard was investigated for each climate zone according to three metrics, seasonal peak load shifting, seasonal peak load reduction, and total annual cooling and heating load reduction. Peak load shifting represents the ability of the PCM composite layer to shift the peak load to a later time in the day, thereby reducing the load on the electrical grid at peak times. Peak load reduction is the ability of the PCM layer to reduce the maximum heating or cooling load in a given diurnal period. The total annual cooling load is measured as the amount of heat flux into the building during the cooling season. Similarly, the annual heating load is the amount of heat flux out of the building during the heating season. In Minneapolis, MN, climate zone 1, the cooling season was defined as June through August based on the following criterion: if the majority of days in the month require cooling, that month is

included in the cooling season; all other months belong to the heating season. In Louisville, KY, climate zone 3, the cooling season was determined to be May through October. The cooling season for Miami, FL, climate zone 5, was taken to be theentire year since there is no heating season. In the one-dimensional simulation the interior boundary conditions for the heating and cooling seasons were defined as constant temperatures of 20°C and 24°C respectively (Diaconu and Cruceru, 2010). No set point temperature bandwidth was taken into account. (The temperature bandwidth is a temperature range centered on the set point temperature within which acceptable thermal comfort levels are achieved as defined by building occupants).

To generate the necessary data to determine the performance of the PCM composite wallboard, three sets of simulations were run. All simulations were executed for an entire year using the TMY3 boundary conditions. First, a set of baseline simulations of the five building surfaces were run for each climate zone (15 simulations). In these baseline simulations the multi-layered roof and wall systems did not contain a PCM composite layer. Next, simulations with PCM composite wallboard enhanced building envelopes in all three configurations for each climate zone were run (45 simulations). The final set of simulations is similar to the second set but without considering the latent heat storage (45 simulations). In total, 105 simulations were executed to determine the performance of the PCM composite wallboard in climate zones 1, 3, and 5 for each of the three configurations discussed.

In order to understand the energy saving potential of the PCM composite wallboard, the data generated by the simulations discussed above will be presented in

three different variations. First, graphs of the heat flux into the room from a south facing wall in all climate zones will be shown for two four-day periods in both the heating and cooling seasons. From this data average values of peak load reduction and peak load shifting will be quantified. Tables will also be shown with four-day average values of peak load reduction and peak load shifting for all building envelope surfaces. Second, annual cooling and heating season percentage load reduction will be presented. The percentage load reduction due to sensible energy storage and latent energy storage will be differentiated in this analysis to directly quantify the effect from the PCM. Third, the annual load reduction in kWh will be presented for all climate zones studied with special attention to Louisville, KY, which displayed the highest energy saving potential.

B. Peak Load Shifting and Reduction

The heat flux profiles for the three PCM placement scenarios for the cooling season in the south facing walls for each climate zone are shown in Figures 18, 19, and 20. The outside ambient temperature profile is also shown. The heat flux in Figures 18, 19, and 20 is reported at the interior of the multi-layered wall system where the wall interfaces with the room air. It is clear that the heat flux peaks and troughs lag the peaks and troughs of the ambient temperature and cases 2 and 3 have the most significant changes in peak load reduction and load shifting from the baseline case with no PCM composite.

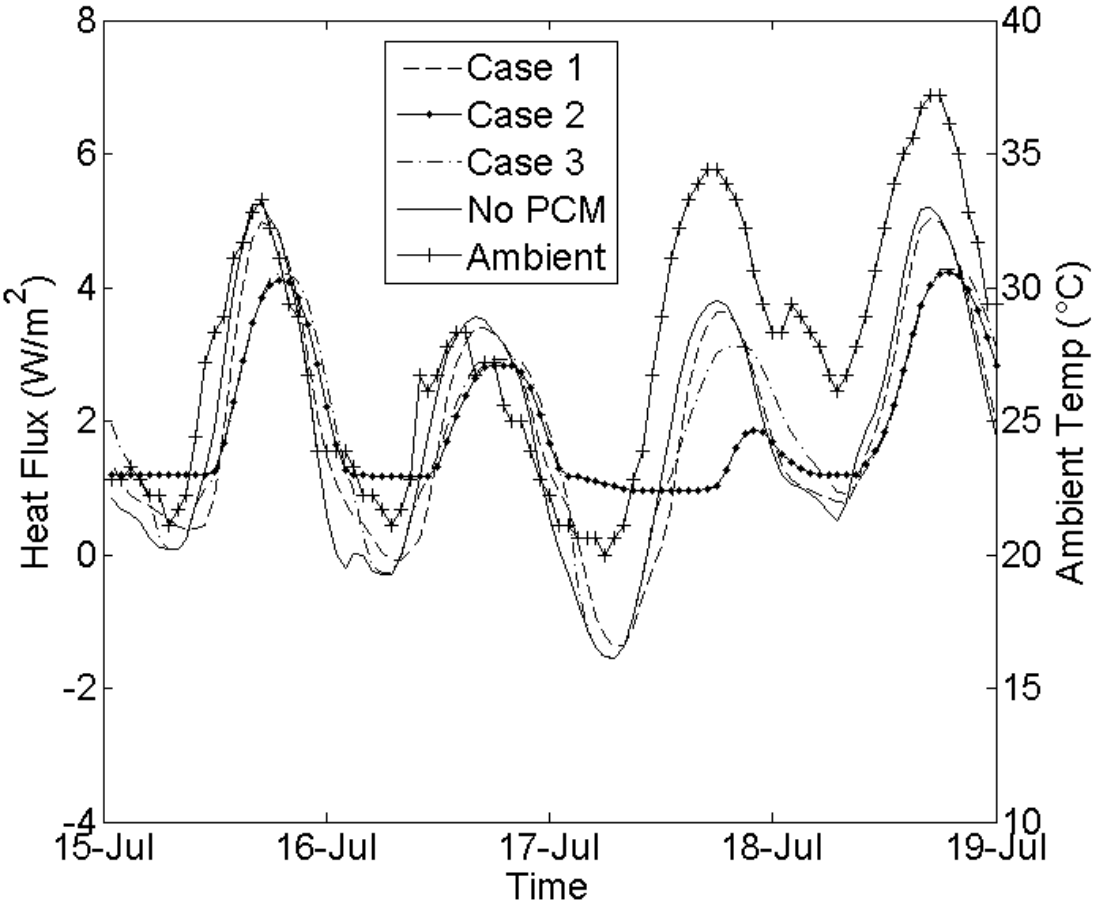

FIGURE 18 – Cooling Season Heat Flux Profiles in the South Wall in Climate Zone 1, Minneapolis, MN

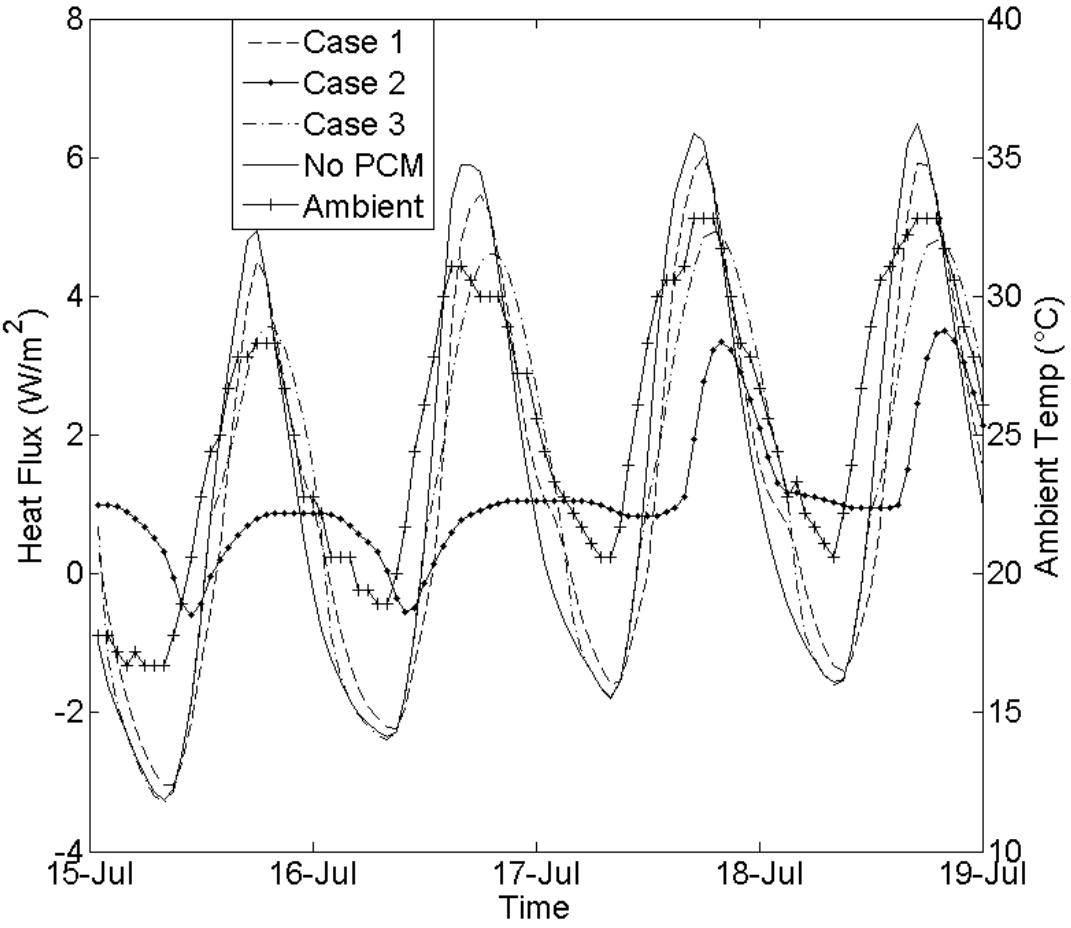

FIGURE 19 – Cooling Season Heat Flux Profiles in the South Wall in Climate Zone 3, Louisville, KY

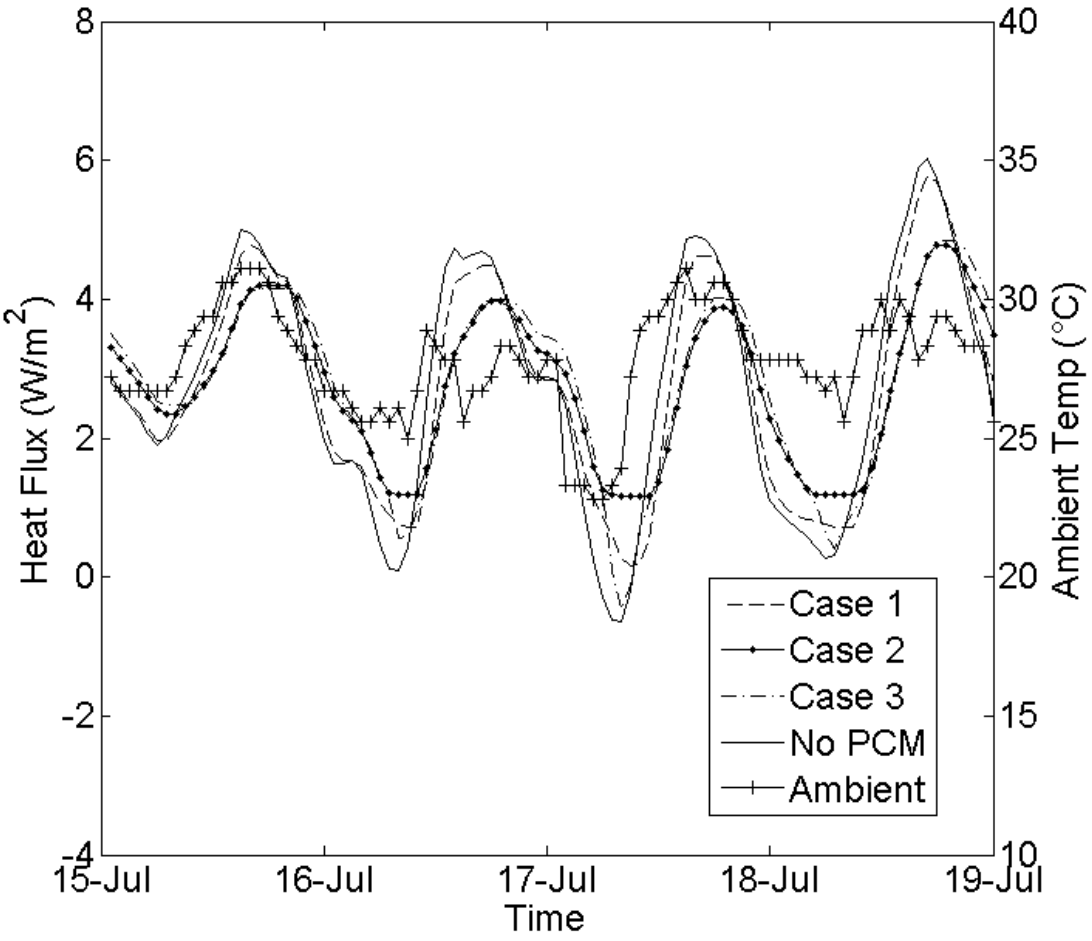

FIGURE 20 – Cooling Season Heat Flux Profiles in the South Wall in Climate Zone 5, Miami, FL

Tables VI, VII, and VIII show the average peak load shifting and peak load reduction for each building surface in climate zones 1, 3, and 5 respectively over the same four day period of July 15th to 18th.

TABLE VI

AVERAGE PEAK LOAD SHIFTING/REDUCTION IN CLIMATE ZONE 1 FROM JULY 15th TO 18th

Minneapolis, MN						
	Peak Reduction (%)			Load Shift (hr)		
	Case 1	Case 2	Case 3	Case 1	Case 2	Case 3
North	3.70	22.90	20.60	0.75	1.25	1.25
South	4.30	27.90	18.30	0.25	2.50	1.50
East	5.70	23.80	19.90	0.50	3.50	4.00
West	6.30	25.00	24.20	0.50	1.00	1.50
Roof	8.00	11.90	33.00	0.75	1.25	3.25

TABLE VII

AVERAGE PEAK LOAD SHIFTING/REDUCTION IN CLIMATE ZONE 3 FROM JULY 15th TO 18th

Louisville, KY						
	Peak Reduction (%)			Load Shift (hr)		
	Case 1	Case 2	Case 3	Case 1	Case 2	Case 3
North	6.27	62.50	18.10	1.00	3.75	1.75
South	7.40	64.60	24.40	0.50	2.75	1.75
East	13.30	53.20	29.50	1.00	6.00	4.50
West	4.10	40.80	28.10	0.50	1.25	1.50
Roof	8.10	15.30	42.30	0.50	1.00	2.75

TABLE VIII

AVERAGE PEAK LOAD SHIFTING/REDUCTION IN CLIMATE ZONE 5 FROM JULY 15th to 18th

Miami, FL						
	Peak Reduction (%)			Load Shift (hr)		
	Case 1	Case 2	Case 3	Case 1	Case 2	Case 3
North	4.00	14.30	14.40	0.25	2.50	2.50
South	4.90	18.40	17.60	1.00	2.50	2.25
East	5.70	20.70	20.20	0.50	2.75	2.50
West	4.00	17.60	18.70	0.50	1.00	1.25
Roof	6.50	9.10	33.50	0.75	1.00	2.50

This analysis shows significant peak load reduction and load shifting potential for all three climate zones studied. Considering the walls in climate zones 1 and 3, the case 2 configuration outperforms cases 1 and 3. In this configuration, the case 2 scenario PCM composite location amplifies the PCM performance by allowing more of the heat passing through the envelope to be stored as both latent and sensible heat and not passed further through the wall. While the maximum amount of potential thermal energy storage is constant across all three cases, the case 2 configuration displays the best performance. Considering the walls in climate zone 5, the warmest of the climates studied, the case 2 and 3 scenarios are very similar in their peak load shifting and peak load reduction performance. The higher average temperature in this warm climate results in less effective thermal energy storage by latent heat towards the exterior of the building envelope.

Unlike the walls for which the optimal PCM composite location is in the middle of the wall (case 2 configuration has the best performance), for the roof, the case 3 configuration performs the best in all climate zones, as shown in Tables VI, VII, and VIII. This is partially due to the relatively low thermal resistance preceding the capacitive PCM roof layer, leading to higher temperatures throughout the exterior layers of the multi-layered roof. The percentage difference between the R-values of the roof and the walls augmented with PCM composite is approximately 24%, where the wall has the higher R-value.

As the above results indicate, the PCM composite placement within the building envelope affects the performance of the latent heat storage component by limiting the exposure of the PCM layer to the full range of diurnal temperatures. In this way the extent of the melting and solidification of the material throughout a typical diurnal cycle is subjected to a different set of temperature ranges as a function of location. To further develop this idea Figures 21, 22, and 23 show the liquid phase fractions of the outermost node of the PCM composite layer in the south wall for all three cases in each climate zone for the same four day cooling season period.

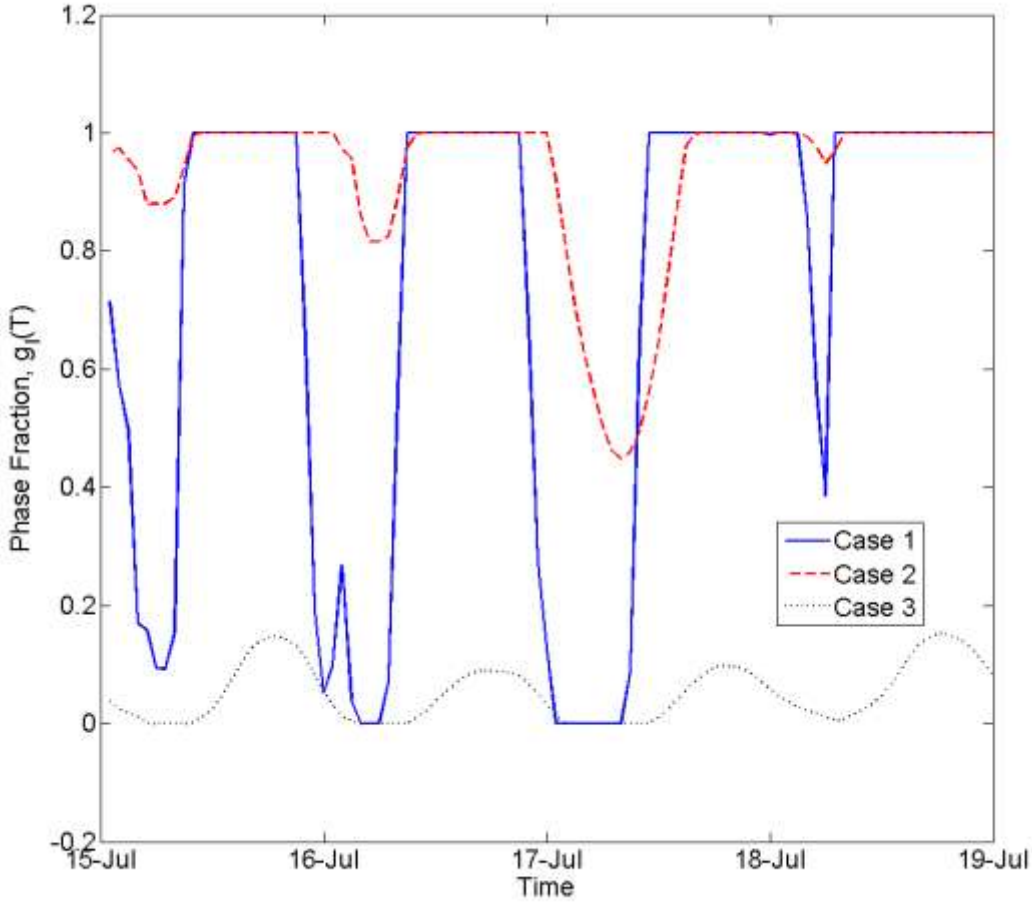

FIGURE 21 – Liquid Phase Fraction Evolution in the South Wall in Climate Zone 1, Minneapolis, MN

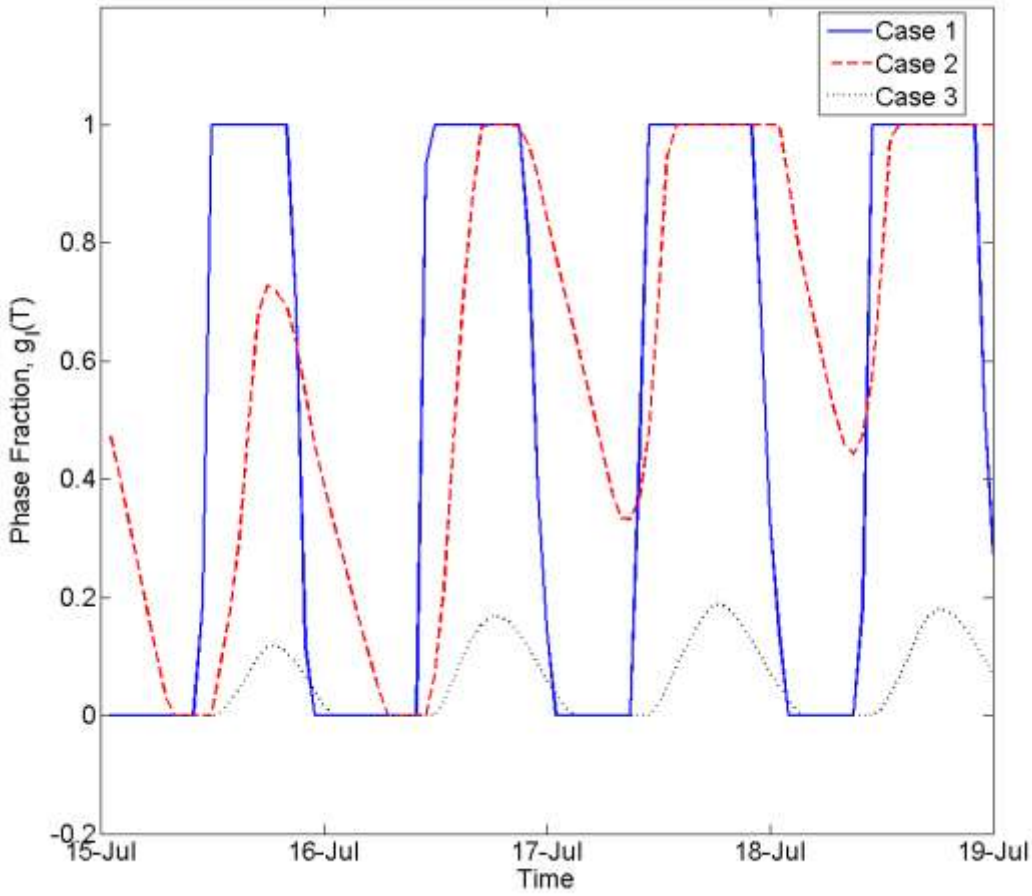

FIGURE 22 – Liquid Phase Fraction Evolution in the South Wall in Climate Zone 3, Louisville, KY

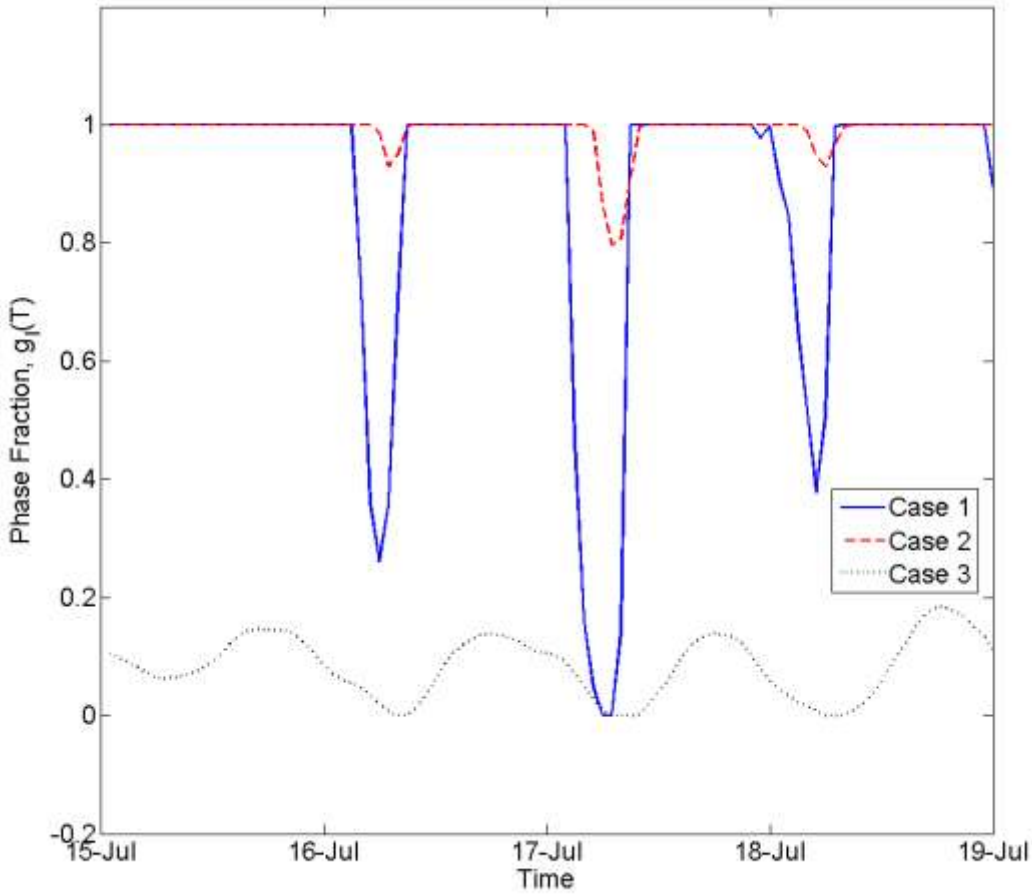

FIGURE 23 – Liquid Phase Fraction Evolution in the South Wall in Climate Zone 5, Miami, FL

For the case 1 scenarios in all the climates studied the PCM undergoes the largest amount of phase transitioning through each diurnal cycle. This is a desirable result in which a maximum amount of latent heat storage is achieved. However, an equivalent performance to the peak load reduction and peak load shifting of cases 2 and 3 is not met. Cases 2 and 3 ultimately store less latent heat but have a greater effect on the peak load and peak load shifting. This is a result of the case 2 and 3 scenarios having the benefit of

thermal resistance layers between the PCM and the exterior boundary conditions, resulting in a smaller ΔT across the capacitive PCM layer. This leads to the storage of a higher percentage of the total thermal energy passing through the PCM layers in the case 2 and 3 scenarios compared to case 1. Furthermore, the phase transitioning for the cooling season is limited by the nighttime temperatures. With higher nighttime temperatures leading to insufficient nighttime cooling, the PCM in case 2 remains primarily in the liquid state, as seen in Figures 21 and 23. The diurnal temperature swings in climate zone 3 over this four day period were better optimized for PCM performance in this temperature range, evident from the heavily transitioning liquid phase fraction in Figure 22.

The heat flux profiles for the three PCM composite placement scenarios for the heating season are shown in Figures 24 and 25 for a south wall in climate zones 1 and 3 only. Climate zone 5 does not require significant amounts of heating and is therefore not considered in the heating season analysis.

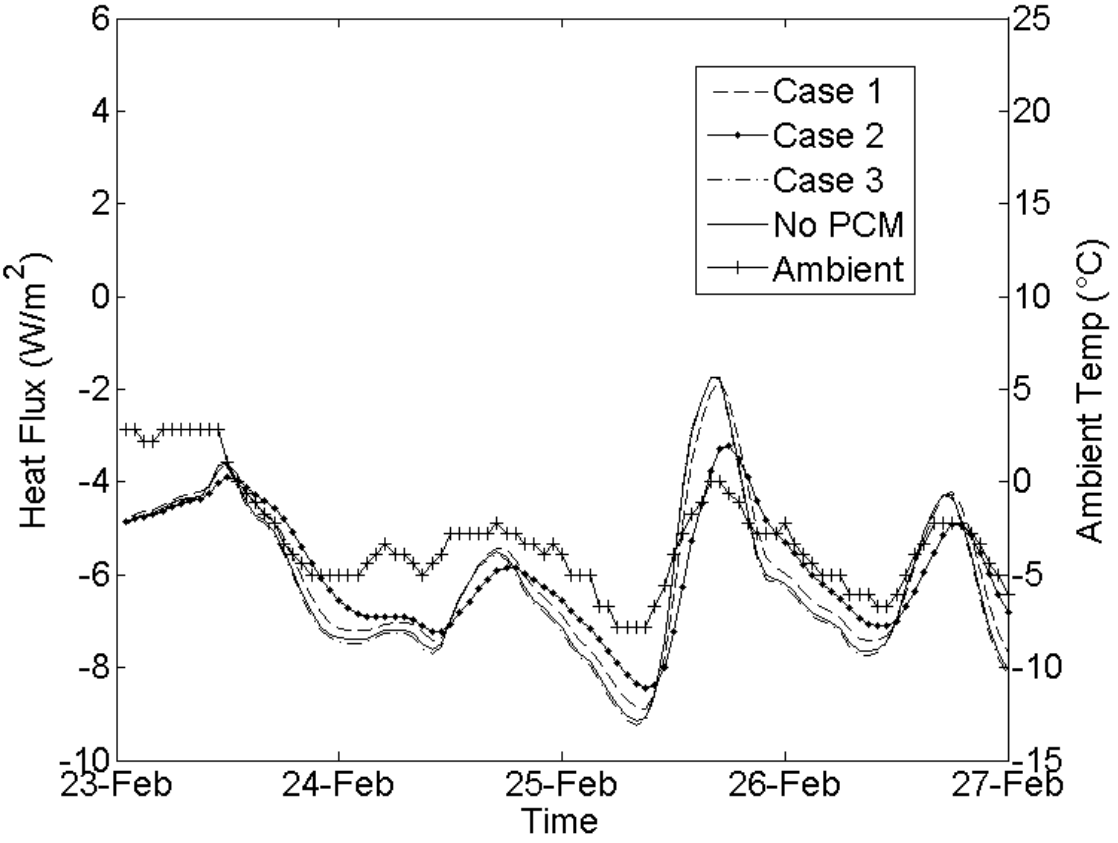

FIGURE 24 – Heating Season Heat Flux Profiles in the South Wall in Climate Zone 1, Minneapolis, MN

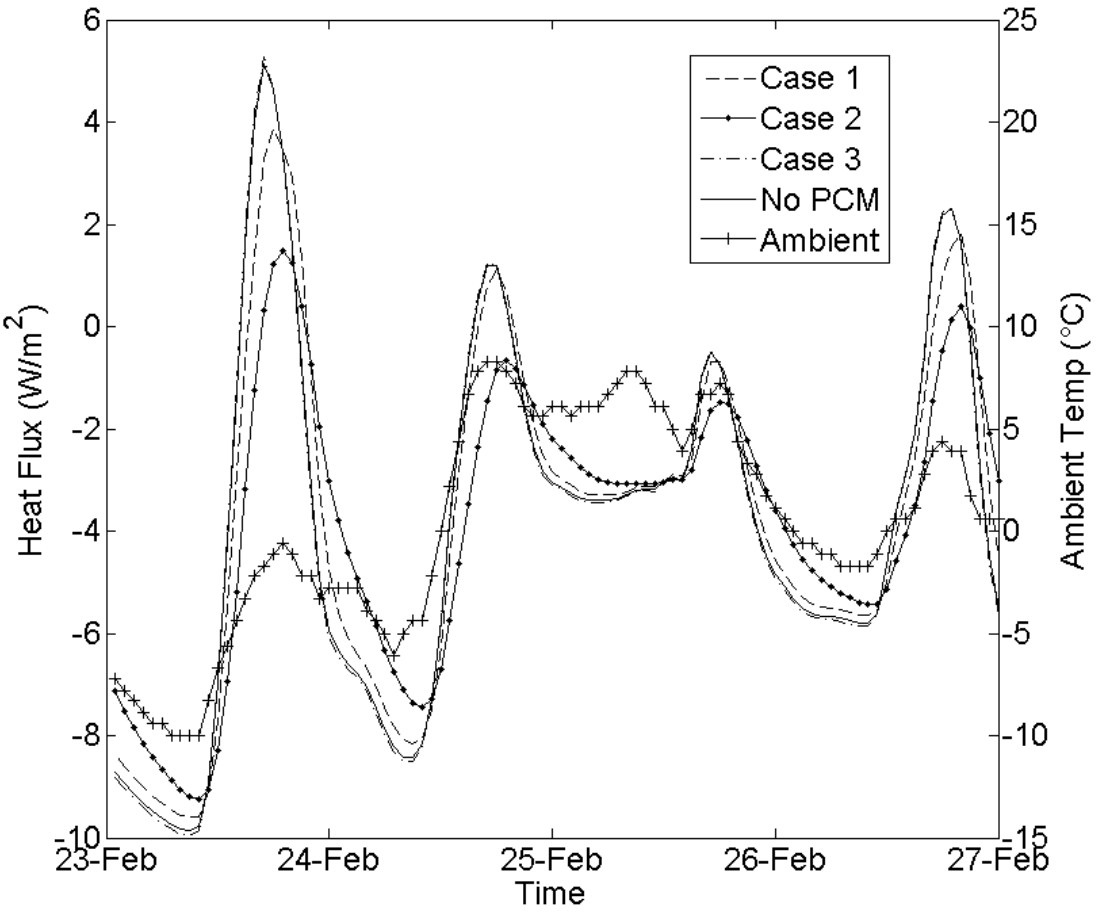

FIGURE 25 – Heating Season Heat Flux Profiles in the South Wall in Climate Zone 3, Louisville, KY

Figures 24 and 25 show minimal differences between all three PCM composite placement scenarios. The centrally located PCM composite, case 2, exhibits the best performance similar to the cooling season. Tables IX and X show the average peak load shifting and peak load reduction over the four day period from February 23rd to 26th.

TABLE IX

AVERAGE PEAK LOAD SHIFTING/REDUCTION IN CLIMATE ZONE 1 FROM FEBRUARY 23th to 26th

Minneapolis, MN						
	% Peak Reduction			Load Shift (hr)		
	Case 1	Case 2	Case 3	Case 1	Case 2	Case 3
North	2.5	4.6	-1	0.75	1	0
South	2.4	4.8	-1.01	0.5	1	0
East	2.4	4.6	-0.99	0.5	0.75	0
West	2.5	4.8	-1.01	0.75	1	0
Roof	2.3	4.2	5.5	0.5	0.75	0.25

TABLE X

AVERAGE PEAK LOAD SHIFTING/REDUCTION IN CLIMATE ZONE 3 FROM FEBRUARY 23th to 26th

Louisville, KY						
	Peak Reduction (%)			Load Shift (hr)		
	Case 1	Case 2	Case 3	Case 1	Case 2	Case 3
North	2.9	6.2	-1.04	0.25	1	0
South	2.8	8.3	-1.1	0.5	1.5	-0.25
East	2.8	6.2	-1.1	0.75	1.25	0.25
West	2.9	7.4	-1.04	0.5	1.25	0
Roof	5.1	5.4	6.7	0.25	0.75	0.5

The peak load reduction during the heating season is significantly less than that of the cooling season. Due to the phase transition temperature range of the PCM selected, the load shifting and peak load reduction is not due to phase change transition and the

resulting latent heat storage. Instead, as will be discuss later, the load shifting and peak load reduction is due to sensible heat storage.

Figure 26 shows the liquid phase fraction, $g_l(T)$, for the outermost node of the PCM composite layer in the south wall over the same four day heating season period for climate zones 3. In zone 1 the PCM remains solid in all the three cases and in zone 3 the liquid phase fraction remains zero throughout the diurnal cycle in case 2, even though case 2 demonstrates both load shifting and peak load reduction in Table IX. This seems to indicate that the load shifting and peak load reduction achieved is due, primarily, to sensible heat storage. Figure 26 shows that for case 1 in zone 3 the PCM composite undergoes some phase transitioning. This indicates that further investigations of heating season benefits through latent heat storage should focus on PCMs with lower melting temperature ranges.

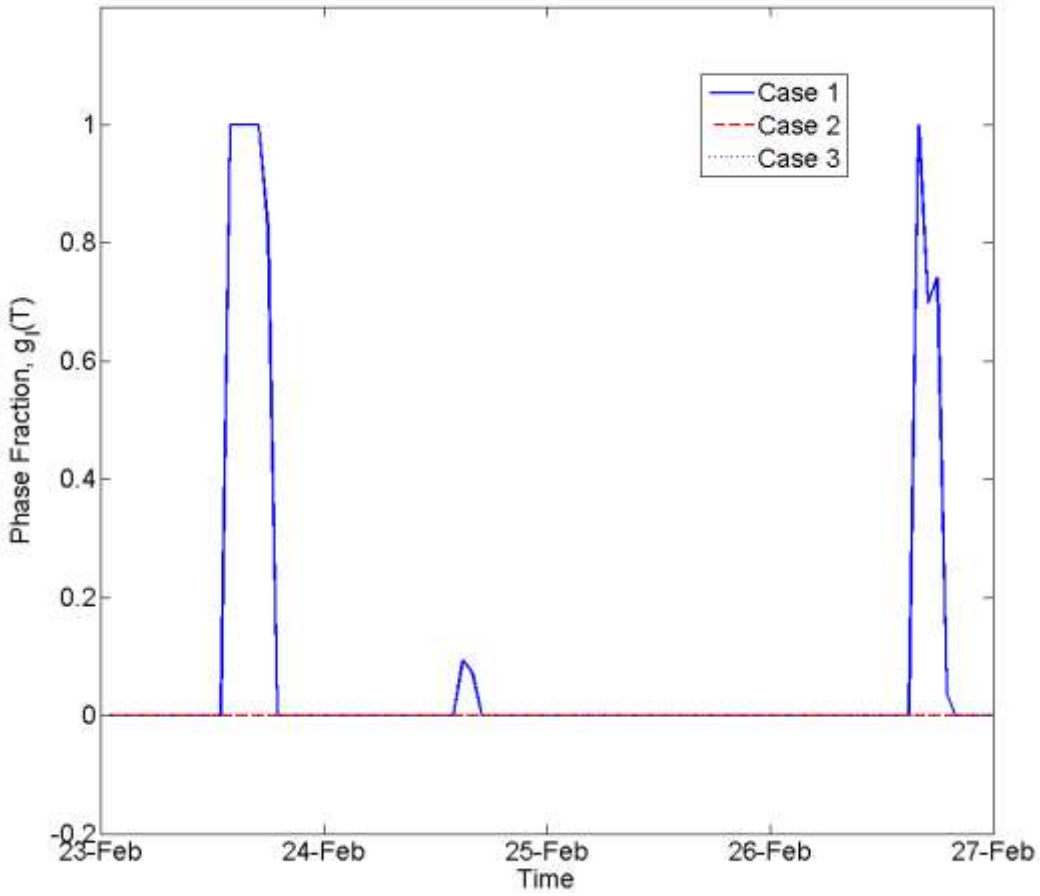

FIGURE 26 – Liquid Phase Fraction Evolution in the South Wall in Climate Zone 3, Louisville, KY

C. Heating and Cooling Season Percentage Load Reduction

The effect of the PCM composite wallboard on decreasing the loads on the conditioned space in both heating and cooling seasons is quantified for the tested building in climate zones 1 and 3 for each PCM composite location. The analysis for climate zone

5 considers only the cooling season due to negligible heating requirements. In addition to measuring the benefits of the PCM enhanced building envelope, the amount of the seasonal load reduction that is due to the sensible heat component alone, i.e. excluding the latent heat effect, is reported.

Tables XI, XII and XIII display the percentage of load reduction in climate zones 1, 3, and 5 respectively compared to a baseline building envelope with no PCM composite layer. The results are reported for the PCM enhanced envelope with and without latent heat storage effects. The resulting load reduction is reported for each building envelope surface over the entire cooling season. In the case 3 scenarios for the walls the increase in the cooling load when only sensible heat storage is considered is due to the decrease in R-value from the original, non-PCM enhanced wallboard to the replacement PCM composite wallboard. The thickness of the original wallboard and the PCM composite wallboard differ by 3.2 mm.

TABLE XI

CLIMATE ZONE 1 COOLING SEASON PERCENTAGE LOAD REDUCTION

Minneapolis, MN						
	Case 1		Case 2		Case 3	
	Total (%)	Sensible only (%)	Total (%)	Sensible only (%)	Total (%)	Sensible only (%)
North	6.73	3.32	32.47	16.60	4.03	-0.68
South	8.13	3.89	37.60	19.26	3.32	-0.65
East	6.98	4.06	30.01	15.77	2.21	-0.68
West	5.40	3.06	28.82	15.90	4.97	-0.75
Roof	4.67	3.68	7.71	4.52	10.10	6.82

TABLE XII

CLIMATE ZONE 3 COOLING SEASON PERCENTAGE LOAD REDUCTION

Louisville, KY						
	Case 1		Case 2		Case 3	
	Total (%)	Sensible only (%)	Total (%)	Sensible only (%)	Total (%)	Sensible only (%)
North	6.03	3.34	20.86	11.92	2.32	-0.62
South	5.80	3.66	21.67	12.90	2.77	-0.71
East	5.63	3.61	17.19	10.91	1.90	-0.66
West	4.77	3.02	19.40	11.79	3.72	-0.73
Roof	3.71	3.32	5.38	3.81	8.09	5.44

TABLE XIII

CLIMATE ZONE 5 COOLING SEASON PERCENTAGE LOAD REDUCTION

Miami, FL						
	Case 1		Case 2		Case 3	
	Total (%)	Sensible only (%)	Total (%)	Sensible only (%)	Total (%)	Sensible only (%)
North	2.60	2.57	3.64	4.57	-0.10	-0.53
South	2.67	2.61	4.27	4.88	-0.28	-0.60
East	2.84	2.75	3.58	4.51	-0.24	-0.56
West	2.40	2.37	4.15	4.70	-0.22	-0.60
Roof	2.88	2.94	3.37	3.06	4.26	3.73

Climate zones 1 and 3 display similar performance with the largest total cooling load reduction in the case 2 scenarios. In both climate zones 1 and 3 more than half of the cooling load reduction is due to the sensible heat storage alone. Recalling Figures 21 and 22, it is clear that the optimal temperature range for full utilization of the selected PCM's latent heat storage capacity is not consistently met in both cases 2 and 3, resulting in less than optimal latent heat storage performance. For the PCM studied here, the optimal diurnal temperature range is from 25°C to 28°C, which would allow the PCM to undergo a complete phase transition. The load reduction performance in climate zone 5 is minimal in all configurations. The PCM implementation in climate zone 5 resulted in significant load shifting and peak load reduction but did not contribute significantly to reducing the total heat transfer through the building envelope in the cooling season. In the case 2 scenario in zone 5 the "sensible only" performance was better than the total performance including phase change effects. This highlights the fact that a PCM with a melting

temperature too low for the climate in question can act as a heat trap during the cooling season. A PCM with a higher phase transition temperature should be selected for study in climate zone 5 for improved cooling season performance.

Tables XIV and XV display the percentage of load reduction in climate zones 1 and 3, respectively, for the entire heating season.

TABLE XIV

CLIMATE ZONE 1 HEATING SEASON PERCENTAGE LOAD REDUCTION

Minneapolis, MN						
	Case 1		Case 2		Case 3	
	Total (%)	Sensible only (%)	Total (%)	Sensible only (%)	Total (%)	Sensible only (%)
North	2.45	2.36	3.00	2.81	-0.93	-0.96
South	2.57	2.41	3.44	3.24	-0.94	-0.98
East	2.46	2.38	3.46	3.15	-0.93	-0.97
West	2.76	2.51	4.34	3.71	-0.77	-0.98
Roof	3.73	3.37	4.56	3.71	4.43	4.20

TABLE XV

CLIMATE ZONE 3 HEATING SEASON PERCENTGE LOAD REDUCTION

Louisville, KY						
	Case 1		Case 2		Case 3	
	Total (%)	Sensible only (%)	Total (%)	Sensible only (%)	Total (%)	Sensible only (%)
North	2.48	2.42	3.61	3.56	-1.02	-1.03
South	3.61	3.01	9.37	8.47	-0.97	-1.12
East	2.55	2.48	4.27	4.19	-1.04	-1.05
West	3.39	2.84	7.07	6.54	-0.97	-1.09
Roof	4.74	3.97	6.35	4.76	6.08	6.03

The additional thermal mass in the building envelope system had more of an effect in the warmer of the climate zones shown, climate zone 3. In both climate zones the case 2 placement scenario results in the highest load reduction. Only a fraction of the heating season savings is due to the latent heat storage of the PCM composite.

D. Annual Load Reduction

The total amount of predicted load reduction in both heating and cooling seasons for the three climate zones studied are shown in Tables XVI and XVII.

TABLE XVI

ANNUAL COOLING LOAD REDUCTION FOR THE WHOLE BUILDING WITH AND WITHOUT LATENT HEAT EFFECT

	Annual Cooling Load Reduction (kWh)					
Climate zone	Case 1		Case 2		Case 3	
	Total	Sensible only	Total	Sensible only	Total	Sensible only
1	80.69	55.97	226.84	124.55	126.34	70.73
3	142.27	112.39	321.63	207.34	219.25	122.61
5	222.55	223.84	283.48	287.07	218.61	180.97

The best total cooling load performance over the entire season is found in climate zone 3. Approximately 35% percent of this load reduction is due to latent heat storage. In climate zone 1 approximately 45% of the load reduction is due to latent heat storage. Although there is a smaller amount of total savings in climate zone 1, the PCM selected for this study has a phase transition temperature range that performs best in this zone on an annual basis. In the case of climate zone 5, the latent heat storage at this phase transition temperature decreases the performance of the additional thermal mass from the PCM composite wallboard in all but the case 3 scenario.

The annual heating load reduction in climate zones 1 and 3 shows less of an effect from the latent heat storage in Table XVII. In the case 2 scenario where the maximum amount of load reduction occurs, approximately 14% and 15% is due to latent heat storage in climate zones 1 and 3 respectively. In order to obtain year round energy savings from latent heat storage in these mid latitude climates, dual layer PCM enhanced building envelopes should be studied.

TABLE XVII

ANNUAL HEATING LOAD REDUCTION FOR THE WHOLE BUILDING WITH AND WITHOUT LATENT HEAT EFFECT

	Annual Heating Load Reduction (kWh)					
Climate zone	Case 1		Case 2		Case 3	
	Total	Sensible only	Total	Sensible only	Total	Sensible only
1	244.02	224.56	315.62	270.53	129.24	117.2
3	144.86	125.12	234.95	199.38	85.23	82.97

Case 2 in climate zone 3, Louisville, KY, shows the best performance with a total annual load reduction of approximately 557 kWh. During the cooling season the load through the walls is reduced by 194 kWh, or 19.7%, and the load through the roof is reduced by 128 kWh, or 8.1%. During the heating season the load through the walls is reduced by 124 kWh, or 5.9%, and the load through the roof is reduced by 111 kWh, or 6.3%. The largest percentage reduction occurs in the walls during the cooling season when the PCM is most active. PCMs with different melt temperatures, varying quantities, and different multi-layered roof systems should be studied in order to improve the load reduction through the walls during the heating season and the roof during both heating and cooling seasons.

VI. CONCLUSION & RECOMMENDATIONS

A finite volume based numerical model was developed and used to solve the one-dimensional, transient heat equation through multi-layered building envelope surfaces. The latent heat storage of the PCM was accounted for with a phase fraction in a latent heat source term. The model was validated against analytical solutions for 1-dinmensional transient conduction through a plane wall with convection on both boundaries and a 1-dimensional transient solution to the two-phase Stefan problem.

The effect of location within a multi-layered wall or roof of a PCM composite wallboard was studied in three climate zones. The boundary conditions are derived from TMY3 weather data for Minneapolis, MN, Louisville, KY, and Miami, FL. The PCM enhanced building envelope performance was identified by comparing the performance of the PCM wallboard against the performance of a building envelope without PCM. It was found that the centrally located PCM composite wallboard performed better than externally and internally located PCM composites in the multilayered wall systems during both the heating and cooling seasons. In the multi-layered horizontal roof systems, a PCM wallboard location on the interior of the building envelope performed best in both heating and cooling seasons. During the heating season, sensible heat storage is primarily responsible for the performance improvements. The temperatures during the heating season within the wall and roof systems are below the phase transition temperature of the chosen PCM for a majority of time.

The results of the study indicate that the use of a PCM composite wallboard within a building envelope in climate zones 1, 3, and 5 can substantially decrease the peak heating and cooling loads and successfully shift the peak cooling loads to later times in the day. The reduction of the cooling season load for the entire building envelope was significant in climate zones 1 and 3 with this PCM phase transition temperature. Over half of the cooling season load reduction was a result of sensible heat storage alone. There was no significant reduction in the cooling season load in climate zone 5. A PCM with a higher phase transition temperature range should be studied for use in climate zone 5.

With respect to peak load reduction, peak load shifting, and annual load reduction the PCM composite wallboard placement scenario that performed best was case 2 in Louisville, KY. The highest peak load reduction was found in the south wall with a four day cooling season average reduction of 64.6%. This scenario was also the best performer in the heating season at an 8.3% peak load reduction. The best cooling season load shifting potential was in the east wall with a four-day average load shift of 6 hours. The combined annual heating and cooling load reduction was greatest in Louisville, KY at 557 kWh followed closely by Minneapolis, MN at 542 kWh. While Louisville, KY saw the largest cooling season load reduction, only 35% was due to latent heat storage compared to 45% in Minneapolis, MN. This indicates that a melt temperature optimized PCM may perform better in the Louisville, KY climate in the case 2 configuration compared to the PCM chosen for this study.

With the completed development of the simulation tool, many interesting studies can be performed to shed additional light on the energy savings potential of PCMs in buildings. Parametric and design of experiment type studies to determine the optimal phase change temperature range, quantity of PCM, and location within building envelopes in any climate zone can be performed. This will lead to knowledge of the best heating and cooling season building envelope layouts and PCM properties in a given climate zone.

Additionally, more advanced building envelope design concepts can be investigated with slight modifications to the numerical model. For example, Diaconu and Cruceru (2010) have studied a building envelope system with two PCM layers of different phase transition temperatures which achieves better year round performance. By replicating that study but using PCMs of heating and cooling season optimized phase change transition temperature ranges and locations, a high performance building envelope system for effective year round performance can be explored.

REFERENCES CITED

ASHRAE, 2001. *2001 AHSRAE Handbook of Fundamentals*, American Society of Heating, Refrigeration and Air-Conditioning Engineers, Atlanta, Georgia, p. 29.28.

Athienitis, A.K., Liu, C., Hawes, D., Banu, D., Feldman, D. 1997. Investigation of thermal performance of a passive solar test-room with wall latent heat storage. *Building and Environment* 32:405-410.

BASF, "Phase Change Materials", 2012, available from http://www.micronal.de/portal/basf/ien/dt.jsp?setCursor=1_290798; accessed 1 Jan. 2012.

BASF, "Micronal PCM®, Intelligent Temperature Management for Buildings", 2009, available from http://www.dispersions-pigments.basf.com/portal/load/fid443847/BASF_Micronal_PCM_Brochure%202009_English.pdf; accessed 6 June 2012.

Bird, R.B., Stewart, W.E., Lightfoot, E.N. 2007. *Transport Phenomena 2nd edition*, New York: John Wiley and Sons, p. 281.

Cabeza, L.F., Castellon, C., Nogues, M., Medrano, M., Leppers, R., Zubillaga, O. 2007. Use of microencapsulated PCM in concrete walls for energy savings. *Energy and Buildings* 39:113-119.

Castellon, C., Gunther, E., Mehling, H., Heibler, S., Cabeza, L.F. 2008. Determination of the enthalpy of PCM as a function of temperature using a heat-flux DSC – A study of different measurement procedures and their accuracy. *International Journal of Energy Research* 32: 1258-1265.

Diaconu, B.M., Cruceru, M. 2010. Novel concept of composite phase change material wall system for year-round thermal energy savings. *Energy and Buildings* 42:1759-1772.

Duffie, J.A., Beckman, W.A. 1991. *Solar engineering of thermal processes*, John Wiley, New York.

EIA (U.S. Energy Information Association), "Total Energy Flow", 2010, available from http://www.eia.gov/totalenergy/data/annual/diagram1.cfm; accessed 3 Mar. 2012.

EIA (U.S. Energy Information Association), "Average Consumption by Energy End Uses", 2005, available from http://www.eia.gov/emeu/recs/recs2005/hc2005_tables/c&e/pdf/tableus14.pdf; accessed 3 Mar. 2012.

EIA (U.S. Energy Information Association), "U.S. Climate Zone Map", 1996, available from http://www.eia.gov/emeu/recs/recs97/zonemap.pdf; accessed 11 June 2012.

EnergyPlus, "EnergyPlus Engineering Reference", 11 October 2010, available from http://apps1.eere.energy.gov/buildings/energyplus/pdfs/engineeringreference.pdf; accessed 11 June 2012.

Fang, Y., Medina, M.A. 2009. Proposed modifications for models of heat transfer problems involving partially melted phase change processes. *Journal of ASTM International* 6:1-20.

Farid, M.M., Khudhair, A.M., Razack, S.A.K., Al-Hallaj, S. 2004. A review on phase change energy storage: materials and applications. *Energy Conversion and Management* 45:1597-1615.

Gunther, E., Hiebler, S., Mehling, H., Redlich, R. 2009. Enthalpy of phase change materials as a function of temperature: required accuracy and suitable measurement methods. *International Journal of Thermophysics* 30:1257-1269.

Halford, C.K., Boehm, R.F. 2007. Modeling of phase change material peak load shifting. *Energy and Buildings* 39:298-305.

Holman, J.P. 1981. *Heat Transfer*, Fifth, New York: Mcgraw-Hill, Inc., p. 191, 272-286.

Incropera, F.P., DeWitt, D.P., Bergman, T.L., Lavine, A.S. 2007, *Introduction to Heat Transfer*, Fifth, Notre Dame: John Wiley and Sons, p. 558.

Khudhair, A.M., Farid, M.M. 2004. A review on energy conservation in building applications with thermal storage by latent heat using phase change materials. *Energy Conversion and Management* 45:263-275.

Kim, E.Y., Kim, H.D. 2005. Preparation and Properties of Microencapsulated Octadecane with Waterborne Polyurethane. Journal of Applied Polymer Science 96:1596-1604.

Kousksou, T., Jamil, A., Zeraouli, Y., Dumas, J.-P. 2006. DSC study and computer modeling of the melting process in ice slurry. *Thermochimica Acta* 448:123-129.

Kuznik, F., David, D., Johannes, K., Roux, J.J. 2011. A review on phase change materials integrated in building walls. *Renewable and Sustainable Energy Reviews* 15:379-391.

Microtek Laboratories Inc., "Standard MicroPCM Products", 2010, available from http://www.microteklabs.com/micropcm_products.html; accessed 6 June 2012.

Nellis, G., Klein, S. 2009. *Heat Transfer*, Cambridge: Cambridge University Press.

NREL (National Renewable Energy Laboratory), "National Solar Radiation Data Base", 2008, available from http://rredc.nrel.gov/solar/old_data/nsrdb/1991-2005/tmy3/; accessed 3 Mar. 2012.

Patankar, Suhas V. 1980. *Numerical Heat Transfer and Fluid Flow*, New York: Hemisphere Publishing Corporation.

Solomon, A. D. 1979. An Easily Computable Solution to a Two-phase Stefan Problem. *Solar Energy* 23:525-528.

Stovall, T.K., Tomlinson, J.J. 1995. What are the potential benefits of including latent storage in common wallboard? *Transactions of the ASME* 117:318-325.

Voller, V.R., Swaminathan, C.R. 1990. Fixed grid technique for phase change problems: a review. *International Journal for Numerical Methods in Engineering* 30:875-898.

Wilkes, K.E. 1989. *Model for Roof Thermal Performance*. Oak Ridge National Laboratory, Report ORNL/CON-274.

Zalba, B., Marin, J.M., Cabeza, L.F., Mehling, H. 2003. Review on thermal energy storage with phase change: materials, heat transfer analysis and applications. *Applied Thermal Engineering* 23:251-283.

VITA

Stephen David Zwanzig

2110 Cherokee Pkwy Apt. G ■ Louisville, KY ■ (502) 762-5964
stephenzwnzig@gmail.com

EDUCATION

M.Eng. in Mechanical Engineering – *with Honors* — Expected July 2012
J.B. Speed School of Engineering, University of Louisville — GPA 4.0

B.S. in Mechanical Engieering – *with High Honors* — May 2012
J.B. Speed School of Engineering, University of Louisville — GPA 3.6

B.S. in Mathematics — December 2007
College of Arts & Sciences, University of Louisville — GPA 3.5

Skills and coursework:

C/C++	Matlab/Simulink	HVAC
FORTRAN	ANSYS 13.0	Mechatronics
Maple 15	BEOpt	SolidWorks

RESEARCH EXPERIENCE

University of Louisville CFD Laboratory — Louisville, KY
Graduate Research Assistant — August 2010 – Present

Research involves the development of a numerical model for heat transfer through multi-layered building envelope systems incorporating phase change material (PCM) composites. PCM thermal properties were characterized using DSC. A design of experiments approach is used to optimize the PCM composite performance.

Oak Ridge National Laboratory — Oak Ridge, TN
HERE Program Participant — June – August 2011

Research involved studying the effect of climate zone on cool roof performance using a custom simulation tool. Using a solar spectrum reflectometer, the impact of updating the ASTM C1549 standard on Cool Roof Rating Council sponsored products was quantified. The effect of this change on predicted energy savings of cool roofs was shown.

ENGINEERING EXPERIENCE

SCHOTT North America Inc. Louisville, KY
Engineering Co-op January – May 2009

Primary duties involved working on a team to design a production process/machine for transparent armor under a US DoD DX-rated contract. Also, designed and executed reliability experiments on company products and coordinated process improvement installations on the production line.

Boulard Designs International Louisville, KY
Industrial Design Technician May – November 2006

Daily work consisted of creating solid models and multi-view drawings of appliance/machine parts using SolidWorks. Ensured that all injection molded part designs met the standards of manufacturability and worked directly with customers to ensure all needs were satisfied.

ACTIVITIES AND HONORS

- 2nd in poster competition 2011 Kentucky Statewide Workshop: Energy Efficiency & Renewable Energy
- Rebecca and Henry P. Conn Graduate Fellowship, 2011-2012
- Trustees Scholarship, 2003-2007